

Comparing Bayesian and traditional end-member mixing approaches for hydrograph separation in a glacierized basin

Zhihua He^{1,‡}, Katy Unger-Shayesteh³, Sergiy Vorogushyn¹, Stephan M. Weise⁴, Doris Duethmann⁵, Olga
Kalashnikova⁶, Abror Gafurov¹, Bruno Merz^{1,2}

¹GFZ German Research Centre for Geosciences, Section Hydrology, Telegrafenberg, Potsdam,
Germany.

²University of Potsdam, Institute for Environmental Sciences and Geography, Potsdam, Germany

³Now at German Aerospace Center (DLR), International Relations, Linder Höhe, Cologne, Germany

⁴UFZ Helmholtz Centre for Environmental Research UFZ, Department Catchment Hydrology, Halle
Germany

⁵Institute of Hydraulic Engineering and Water Resources Management, Vienna University of
Technology (TU Wien), Vienna, Austria

⁶CAIAG Central Asian Institute of Applied Geosciences, Department Climate, Water and Natural
Resources, Bishkek, Kyrgyzstan

[‡]Now at Centre for Hydrology, University of Saskatchewan, Saskatoon, Saskatchewan, Canada

Abstract

Tracer data have been successfully used for hydrograph separation in glacierized basins. However, uncertainties in the hydrograph separation are large in these basins, caused by the spatio-temporal variability in the tracer signatures of water sources, the uncertainty of water sampling and the mixing model uncertainty. In this study, we used electrical conductivity (EC) measurements and two isotope signatures ($\delta^{18}\text{O}$ and $\delta^2\text{H}$) to label the runoff components, including groundwater, snow and glacier meltwater, and rainfall, in a Central Asia glacierized basin. The contributions of runoff components (CRC) to the total runoff, as well as the corresponding uncertainty, were quantified by two mixing approaches: a traditional end-member mixing approach (abbreviated as EMMA) and a Bayesian end-member mixing approach. The performance of the two mixing approaches was compared in three seasons, distinguished as cold season, snowmelt season and glacier melt season. Results show that: 1) The Bayesian approach generally estimated smaller uncertainty ranges for the CRC compared to the EMMA. 2) The Bayesian approach tended to be less sensitive to the sampling uncertainties of meltwater than the EMMA was. 3) Ignoring the model uncertainty caused by the isotope fractionation likely led to an overestimated rainfall contribution and an underestimated meltwater share in the melt seasons. Our study provides the first comparison of the two end-member mixing approaches for hydrograph separation in glacierized basins, and gives insights for the application of tracer-based mixing approaches for similar basins.

1. Introduction

Glaciers and snowpack store a large amount of fresh water in glacierized basins, thus providing an important water source for downstream human societies and ecosystems (Barnett et al., 2005; Viviroli et al., 2007; He et al., 2014; Penna et al., 2016). Seasonal meltwater and rainfall play significant roles in shaping the magnitude and timing of runoff in these basins (Rahman et al., 2015; Pohl et al., 2017). Quantifying the seasonal contributions of the runoff components (CRC), including groundwater, snowmelt, glacier melt and rainfall, to the total runoff is therefore highly needed for the understanding of the dynamics of water resources in glacierized basins under the current climate warming (La Frenierre and Mark, 2014; Penna et al., 2014; He et al., 2015).

The traditional end-member mixing approach (abbreviated as EMMA) has been widely used for hydrograph separation in glacierized basins across the world (Dahlke et al., 2014; Sun et al., 2016a; Pu et al., 2017). For instance, studies in the Italian glacierized Alpine catchments indicate the successful application of the EMMA to estimate the proportions of groundwater, snow and glacier meltwater based on water stable isotopes and electric conductivity (EC) (e.g., Chiogna et al. 2014, Engel et al. 2016 and Penna et al. 2017). Li et al. (2014) confirmed significant contributions of snow and glacier melt runoff to total runoff in the Qilian Mountains using EMMA. Maurya et al. (2011) reported the contribution of glacial ice meltwater to the total runoff in a Himalayan basin on $\delta^{18}\text{O}$ and EC, using a three-component EMMA.

However, uncertainties in CRC quantified by EMMA in glacierized basins are typically high (Klaus and McDonnell, 2013; Rahman et al., 2015), because of the following reasons: (1) The catchment elevation generally extends over a large range, leading to strong spatial variability in climate forcing (precipitation and temperature) and the tracer signatures of water sources; (2) The number of end-member water sources for runoff is typically high, additionally including snow and glacier meltwater; (3) Water sampling in high-elevation glacierized catchment is difficult due to the logistical limitations, resulting in small sample sizes for the application of EMMA. Uncertainties in CRC quantified by the EMMA can be categorized into statistical uncertainty and model uncertainty. Statistical uncertainty refers to the spatio-temporal variability of the tracer signatures, sampling uncertainty and laboratory measurement error (Joerin et al., 2002). Model uncertainty is determined by the assumptions of the EMMA, which might not agree with reality (Joerin et al., 2002; Klaus and McDonnell, 2013). For example, the fractionation effect on isotope ratios caused by evaporation during the mixing process can result in significant errors given the constant tracer assumption in the EMMA (Moore and Semmens, 2008).

The Gaussian error propagation technique has been typically applied along with EMMA to estimate the statistical uncertainty for hydrograph separation, assuming the uncertainty associated with each source is independent from the uncertainty of other sources (Genereux, 1998; Pu et al., 2013). The spatio-temporal variability of the tracer signatures is estimated by multiplying the t values of the Student's t distribution at the selected significance level with the standard deviations (Sd) of the measured tracer signatures (Pu et al., 2013; Penna et al., 2016; Sun et al., 2016b). Although this approach has been successfully used in various glacierized basins, some recurring issues remain. These include (1) inappropriate estimation of the variability of tracer signatures of water sources when only few water samples are available (Dahlke et al., 2014). The used Sd values of the measured tracer signatures likely fail to represent the variability of tracer signatures of individual water sources across the basin, due to the small water sample sizes; (2) The correlation of tracer signatures and runoff components are inevitably ignored, due to the assumption of independence of the multiple uncertainty sources. The correlation between $\delta^{18}\text{O}$ and $\delta^2\text{H}$ of each water source, as well as the interaction between runoff components could provide additional constraints on the uncertainty in the quantification of runoff components, which however are typically ignored in the Gaussian error propagation technique. Further, the model uncertainty caused by the fractionation effect on isotope ratios during the mixing process is also often ignored.

The Bayesian end-member mixing approach (abbreviated as Bayesian approach) shows the potential to estimate the proportions of individual components to the mixing variable in a more rigorous statistical way (Parnell et al., 2010). For hydrograph separation, the tracer signatures of the water sources are first assumed to obey specific prior distributions. Their posterior distribution are then obtained by updating the prior distributions with the likelihood observations derived from water samples. In the last step, CRC to the total runoff are estimated based on the balance of the posterior tracer signatures. The posterior distributions of the CRC are typically estimated in a Markov Chain Monte Carlo (MCMC) procedure. In the Bayesian approach, both the statistical and model uncertainties are represented by the posterior distributions of parameters. The parameter uncertainty is estimated based on likelihood observations using MCMC.

Although the Bayesian approach can be applied in cases when the sample sizes are small (Ward et al., 2010), it has been rarely used for hydrograph separation in glacierized basins. To the authors' knowledge, there have been only three studies, including Brown et al. (2006), who conducted the hydrograph separation in a glacierized basin in the French Pyrenees using a three-component Bayesian approach. Further, Cable et al. (2011) quantified the CRC to total runoff

in a glacierized basin in the American Rocky Mountains. They used a hierarchical Bayesian framework to incorporate temporal and spatial variability in the water isotope data into the mixing model. Recently, Beria et al. (2019) used a classic Bayesian approach to estimate the uncertainty in CRC in a Swiss alpine catchment. However, the performance of the Bayesian approach has not been evaluated in comparison to the EMMA. Moreover, the sensitivity of the Bayesian approach to the water sampling uncertainty associated with the representativeness of the water samples caused by the limited sample site and sample size is still not clear. Benefiting from the prior assumptions for changes in isotope signatures during the mixing process, the Bayesian approach bears the potential to estimate the fractionation effect on isotopic signatures (Moore and Semmens, 2008), which however, has not been investigated either.

In this study, we compare EMMA and the Bayesian approach for hydrograph separation in a Central Asia glacierized basin, using water isotope and EC measurements. In Central Asia, glacierized catchments provide important fresh water supply for downstream cities and irrigated agriculture. Quantifying the contributions of multiple runoff components to total runoff is important for understanding the dynamics of water resource availability at the regional scale. However, uncertainty in the quantification of runoff components in the glacierized catchments are particularly large as mentioned before. Our research questions are two-fold: 1) How do EMMA and Bayesian approaches compare with respect to the quantification of CRC? 2) What is the influence of the different uncertainty sources (including variability of the tracer signatures, sampling uncertainty, and model uncertainty) on the estimated CRC in the two mixing approaches?

The paper is organized as follows: Details on the study basin and water sampling are introduced in Section 2; Assumptions of the two mixing approaches are described in Section 3; Section 4 estimates the CRC, as well as the corresponding uncertainties; Discussion and conclusion finalize the paper in Sections 5 and 6, respectively.

2. Study area and data

2.1 Study area

Located in Kyrgyzstan, Central Asia, the Ala-Archa basin drains an area of 233 km², (Fig. 1), and glaciers cover around 17% of the basin area. The elevation of the study basin extends from 1560 m to 4864 m a.s.l., and the elevation range of the glacierized area extends from 3218 to 4857 m a.s.l., with about 76% located between 3700 and 4100m a.s.l.. The Golubin glacier has an area of ~5.7 km² and extends over an elevation range from 3232 to 4458 m a.s.l. (Fig. 1). Both the elevation range and the mean elevation (3869 m a.s.l.) of the Golubin glacier are close to those of the entire glacierized area (mean elevation is 3945 m a.s.l.). The

Golubin glacier represents about 14.4% of the entire glacierized area, while its elevation range covers around 95.6% of the entire glacier range. The annual mean precipitation and air temperature measured at the Baitik meteorological station during 2012-2017 are 538 mm yr⁻¹ and 7.2 °C, respectively. The mean daily streamflow during 2012-2017 is about 6.3 m³/s (Fig. S1). The seasonal dynamics of runoff in the river play an important role in the water availability for downstream agricultural irrigation. The generation of snow and glacier melt runoff generally shows the largest effect on the runoff seasonality (Aizen et al., 2000; Aizen et al., 2007). In particular, the snowmelt runoff mainly occurs in the warm period from early March to middle September, and the glacier melt typically generates runoff from the high-elevation areas during July to September (Aizen et al., 1996; He et al., 2018; He et al., 2019). We subsequently defined three runoff generation seasons as follows. Cold season: from October to February, in which the streamflow is fed mainly by groundwater and to a smaller extent by snowmelt and rainfall; Snowmelt season: from March to June, in which the streamflow is fed chiefly by snowmelt and groundwater and additionally by rainfall; Glacier melt season: from July to September, in which the streamflow is fed by significant glacier melt and groundwater, rainfall and snowmelt.

Two meteorological stations (Fig. 1), i.e., Alplager (at elevation of 2100 m a.s.l.) and Baitik (at elevation of 1580 m a.s.l.), have been set up in the basin since the 1960s to collect daily precipitation and temperature data. The Ala-Archa hydrological station has been set up at the same site of the Baitik meteorological station to collect daily average streamflow data since the 1960s. The dynamics of glacier mass balance and snow mass balance in the accumulation zone have been surveyed in summer field campaigns through 2012-2017. Daily precipitation, temperature and streamflow measured at the basin outlet during 2012-2017, are presented in Fig. S1 in the supplement file.

2.2 Tracers data

Since July of 2013, stream water samples have been collected weekly by local station operators, from the river channel close to the Alplager and Baitik meteorological sites, using pure 50 ml high-density polyethylene (HDPE) bottles (He et al., 2019). The sampling time slightly varied around noon every Wednesday. Precipitation samples were collected during 2012-2017 at four sites across the basin (Fig. 1). At the Alplager and Baitik meteorological sites, the precipitation samples were first collected from fixed rain collectors (immediately after the rainfall/snowfall events), and then accumulated in two indoor rain containers over one month. The mixed water in the containers were then sampled for isotopic analysis every month. The indoor rain containers were filled with thin mineral oil layers for monthly precipitation accumulation and stored in cold places. Additionally, two plastic rain collectors PALMEX

(similar to Gröning et al., 2012), specifically designed for isotopic sampling to prevent evaporation, were set up at elevations of 2580 m a.s.l. and 3300 m a.s.l. to collect precipitation in high-elevation areas (Fig. 1). Precipitation samples were collected monthly from these two rain collectors during the period from May to October when the high-elevation areas were accessible.

Glacier meltwater was sampled during the summer field campaigns in each year of 2012-2017. Samples of meltwater flowing on the Golubin glacier in the ablation zone and at the glacier tongue were collected by pure 50 ml HDPE bottles and then stored in a cooling box (Fig. 1, the elevation of the sampling sites ranges from 3280 m to 3805 m a.s.l.). We only collected glacier meltwater samples from the Golubin glacier due to the logistic limitations in the remaining glacierized area. Snow samples were collected from early March to early October during 2012-2017, as the sampling sites are generally not accessible due to the heavy snow accumulation in the remaining months. The elevation of the multiple snow sampling sites ranges from 1580 m to 4050 m a.s.l. (Fig. 1). The whole snow profile at each sampling site was collected through drilling a 1.2 m pure plastic tube into the snowpack. The snow in the whole tube were then collected by plastic bags and stored in a cooling box. After all the snow in the plastic bags melted out, the mixed snow meltwater samples were then collected by pure HDPE bottles. Groundwater samples were also collected through March to October during 2012-2017, from a spring draining to the river (Fig. 1, 2400 m a.s.l.) using pure HDPE bottles. The spring is located at the foot of a rocky hill, around 60 meters away from the river channel.

All samples were stored at 4 °C and then delivered to the laboratory at Helmholtz Center for Environmental Research (UFZ) in Halle of Germany by flight. Isotopic compositions of water samples were measured using a Laser-based infrared spectrometry (LGR TIWA 45, Picarro L1102-i). A regular calibration has been carried out to minimize the memory effect. The measurement precisions of both LGR TIWA 45 and Picarro L1102-i for $\delta^{18}\text{O}$ and $\delta^2\text{H}$ are $\pm 0.25\text{‰}$ and $\pm 0.4\text{‰}$, respectively, after the calibration against the common VSMOW standard. We used the Hanan Instruments HI-9813 PH EC/TDS portable meter to measure the EC values of water samples, with a measurement precision of 0.1 $\mu\text{S/cm}$. EC data has been widely used for hydrograph separation, due to its easy use and quick measurement. While EC is not a conservative tracer, this may have only small effects on the application of hydrograph separation at the catchment scale. Abnormal isotopic compositions caused by evaporation and abnormal EC values caused by impurities were discarded. We used threshold values to identify abnormal values of $\delta^{18}\text{O}$ and EC located far away from the sample clusters. For $\delta^{18}\text{O}$, sample

values higher than 5‰ were excluded. For EC, sample values higher than 210 µs/cm were excluded. Tracers data of individual water sources at the sampled date are presented in Fig. S1.

3. Methodology

The hydrograph separation is carried out in each of the three seasons (i.e., cold season, snowmelt season and glacier melt season). Water samples collected in the period from 2012 to 2017 are split into each of the three seasons for the hydrograph separation. The CRC estimated by the mixing approaches refer to the mean contributions in each of the three seasons during the period of 2012-2017. The mixing approaches applied for the hydrograph separation in each season are summarized in Table 2. Considering the groundwater and snowmelt samples were rarely collected in the cold season, we used all available groundwater and snowmelt samples from the three seasons for hydrograph separation in the cold season. Tracer signatures of rainfall are assumed as same as the measured tracer signatures of precipitation samples in all the three seasons.

3.1 Traditional end-member mixing approach (EMMA)

The main assumptions of EMMA are as follows (Kong and Pang, 2012): (1) The tracer signature of each runoff component is constant during the analyzed period; (2) The tracer signatures of the runoff components are significantly different from each other; (3) Tracer signatures are conservative in the mixing process. In the cold and snowmelt seasons, a three-component EMMA method (EMMA_3, Table 2) is used. Since the precision of $\delta^{18}\text{O}$ (± 0.25 ‰) measured in the lab is higher than that of $\delta^2\text{H}$ (± 0.4 ‰) and both are strongly correlated, the EMMA_3 is based on $\delta^{18}\text{O}$ and EC. In the glacier melt season, both the EMMA_3 and the four-component EMMA (EMMA_4, Table 2) are used. In the EMMA_3, glacier melt and snowmelt are assumed as one end-member, considering their similar tracer signatures. In the EMMA_4, glacier melt and snowmelt are treated as two end-members separately, and $\delta^{18}\text{O}$ and $\delta^2\text{H}$ are used as two separate tracers. The following equations (Eqs. 1-5) are used to estimate CRC (f_i) and the corresponding uncertainty in the EMMA_3 (Genereux, 1998).

$$\begin{cases} 1 = f_1 + f_2 + f_3, & \text{for water balance} \\ A = A_1 \cdot f_1 + A_2 \cdot f_2 + A_3 \cdot f_3, & \text{for water tracer A} \\ B = B_1 \cdot f_1 + B_2 \cdot f_2 + B_3 \cdot f_3, & \text{for water tracer B} \end{cases} \quad (1)$$

$$f_1 = \frac{AB_2 - AB_3 + A_2B_3 - A_2B + A_3B - A_3B_2}{A_1B_2 - A_1B_3 + A_2B_3 - A_2B_1 + A_3B_1 - A_3B_2} \quad (2)$$

$$f_2 = \frac{AB_3 - AB_1 + A_1B - A_1B_3 + A_3B_1 - A_3B}{A_1B_2 - A_1B_3 + A_2B_3 - A_2B_1 + A_3B_1 - A_3B_2} \quad (3)$$

$$f_3 = \frac{AB_1 - AB_2 + A_1B_2 - A_1B + A_2B - A_2B_1}{A_1B_2 - A_1B_3 + A_2B_3 - A_2B_1 + A_3B_1 - A_3B_2} \quad (4)$$

where the subscripts 1-3 refer to the three runoff components (i.e., groundwater, snowmelt/meltwater and rainfall), and A_1 - A_3 (B_1 - B_3) refers to the mean $\delta^{18}\text{O}$ (EC) values of runoff components. A and B stand for the mean $\delta^{18}\text{O}$ and EC values of the stream water. The mean isotope and EC values of precipitation are calculated as the monthly precipitation weighted average values. Similarly, the mean isotope and EC values of stream water are calculated as the weekly streamflow weighted average values.

Assuming the uncertainty of each variable is independent from the uncertainty in others, the Gaussian error propagation technique is applied to estimate the uncertainty of the CRC (f_1 , f_2 , f_3) using the following equation (Genereux, 1998):

$$W_{f_i} = \sqrt{\left(\frac{\partial f_i}{\partial A_1} W_{A_1}\right)^2 + \left(\frac{\partial f_i}{\partial A_2} W_{A_2}\right)^2 + \left(\frac{\partial f_i}{\partial A_3} W_{A_3}\right)^2 + \left(\frac{\partial f_i}{\partial A} W_A\right)^2 + \left(\frac{\partial f_i}{\partial B_1} W_{B_1}\right)^2 + \left(\frac{\partial f_i}{\partial B_2} W_{B_2}\right)^2 + \left(\frac{\partial f_i}{\partial B_3} W_{B_3}\right)^2 + \left(\frac{\partial f_i}{\partial B} W_B\right)^2} \quad (5)$$

where f_i stands for the contribution of a specific runoff component, and W is the uncertainty in the variable specified by the subscript. For the uncertainty of tracer signatures (W_{A_i} and W_{B_i}), we multiply the Sd values of the measured tracer signatures with t values from the Student's t value table at the confidence level of 95%. The degree of freedom for the Student's t distribution is estimated as the number of water sample for each water source minus one. Analytical measurement errors are not considered in this approach, which, however, are minor compared to the uncertainty generated from tracer variations (Penna et al., 2017; Pu et al., 2017). The *lsqnonneg* function in Matlab is used to solve Eqs. 1-4, which solves the equations in a least squares sense, given the constraint that the solution vector f has nonnegative elements. The EMMA_4 uses the equations similar to Eqs. 1-5. The values of $\delta^{18}\text{O}$ and $\delta^2\text{H}$ are typically correlated for each water source. However, the coefficients representing the correlation between $\delta^{18}\text{O}$ and $\delta^2\text{H}$ vary among the water sources in glacierized catchment, thus providing a basis for the EMMA_4 to quantify four runoff components. When quantifying four runoff components using three tracers, four conservative equations for $\delta^{18}\text{O}$, $\delta^2\text{H}$, EC, and water volume are used (similar to Eq.1). The contributions of runoff components (f), as well as the partial derivatives used to calculate the uncertainty are solved from the four conservative equations using Matlab. However, the solutions are too lengthy to show in the text.

3.2 Bayesian mixing approach

The Bayesian approaches applied for each season are summarized in Table 2. Similar to the EMMA, we apply a three-component Bayesian approach to all seasons, and additionally

a four-component Bayesian approach in the glacier melt season. The three-component Bayesian approach has two types: the Bayesian_3_OHcor approach considers the correlation between $\delta^{18}\text{O}$ and $\delta^2\text{H}$, whereas the Bayesian_3_OHind approach assumes independence. The four-component Bayesian approach also has two types: Bayesian_4_OHcor considering the correlation, and Bayesian_4_OHind assuming independence between $\delta^{18}\text{O}$ and $\delta^2\text{H}$. A Kolmogorov-Smirnov test has been carried out for both isotope and EC tracers of all water sources before the application of Bayesian approaches. The tracer data of runoff components (i.e., rainfall, snowmelt, groundwater and glacier melt) generally pass the normal distribution test at significance levels of p -values > 0.3 , while the tracer data of stream water fail to pass the normal distributions test partly caused by the extreme isotope and EC values (see Figs. S1a-b). The EC data of glacier melt also fail to pass the normal distribution test, which can be caused by the low sample size. Thus, the prior assumptions for the Bayesian approaches are listed as follows (similarly to Cable et al. 2011): In approaches considering the correlation between $\delta^{18}\text{O}$ and $\delta^2\text{H}$, the prior distributions of $\delta^{18}\text{O}$ and $\delta^2\text{H}$ of runoff components are assumed as bivariate normal distributions with means and precision matrix as $\mu^{18}\text{O}$, $\mu^2\text{H}$ and Ω , respectively (Eq. 6a). The precision matrix (Ω , i.e. the inverse of the covariance matrix) for the two isotopes is assumed as Wishart prior (Eq. 6b). When assuming independence between $\delta^{18}\text{O}$ and $\delta^2\text{H}$, the prior distributions of $\delta^{18}\text{O}$ ($\delta^2\text{H}$) of runoff components are assumed as normal distributions with means and variance of $\mu^{18}\text{O}$ and $\lambda^{18}\text{O}$ ($\mu^2\text{H}$ and $\lambda^2\text{H}$, Eqs. 6c-d). The mean values of the isotopes of runoff components (i.e., $\mu^{18}\text{O}$ and $\mu^2\text{H}$) are further estimated by independent normal priors (Eq. 7, Cable et al. 2011), which is assumed to consider the spatial variability of $\mu^{18}\text{O}$ and $\mu^2\text{H}$.

$$\begin{cases} \begin{bmatrix} \delta^{18}\text{O} \\ \delta^2\text{H} \end{bmatrix} \sim \text{Multi_normal} \left(\begin{bmatrix} \mu^{18}\text{O} \\ \mu^2\text{H} \end{bmatrix}, \Omega \right) \end{cases} \quad (6a)$$

$$\Omega \sim \text{Wishart} (2, V) \quad (6b)$$

$$\delta^{18}\text{O} \sim \text{Normal} (\mu^{18}\text{O}, \lambda^{18}\text{O}) \quad (6c)$$

$$\delta^2\text{H} \sim \text{Normal} (\mu^2\text{H}, \lambda^2\text{H}) \quad (6d)$$

$$\mu^{18}\text{O} \sim \text{Normal} (\gamma^{18}\text{O}, \sigma^{18}\text{O}) \quad (7a)$$

$$\mu^2\text{H} \sim \text{Normal} (\gamma^2\text{H}, \sigma^2\text{H}) \quad (7b)$$

where, $\lambda^{18}\text{O}$, $\gamma^{18}\text{O}$ and $\sigma^{18}\text{O}$ ($\lambda^2\text{H}$, $\gamma^2\text{H}$ and $\sigma^2\text{H}$) are parameters used to describe the normal priors of $\delta^{18}\text{O}$ and $\mu^{18}\text{O}$ ($\delta^2\text{H}$ and $\mu^2\text{H}$, see Table 3), which are estimated by likelihood observations. V is a 2*2 unit positive-definite matrix, and '2' stands for the degree of freedom in the Wishart prior distribution.

The priors of EC values of runoff components are assumed as normal distributions (Eq. 8a), with mean ε and variance τ . Similarly, the spatial variability of the mean EC values of

runoff components (ε) are assumed to follow a normal distribution with mean θ and variance ω (Eq. 8b). τ , θ and ω are parameters estimated by likelihood observations (Table 3).

$$\begin{cases} EC \sim Normal(\varepsilon, \tau) \\ \varepsilon \sim Normal(\theta, \omega) \end{cases} \quad \begin{matrix} (8a) \\ (8b) \end{matrix}$$

The prior distributions of stream water are calculated in two steps. First, the prior distributions of $\delta^{18}O$, δ^2H and EC of stream water are assumed as same as those of runoff components in Eqs. 6 and 8a. Second, the mean isotopes ($\mu^{18}O$ and μ^2H) and EC (ε) of stream water are constrained by a mixing model (Eqs. 9a-b), which estimates the isotope and EC mean values of stream water by multiplying the contribution of each runoff component (f_i) with the corresponding mean isotope and EC values of each runoff component (Eq. 9a).

$$\begin{cases} \begin{bmatrix} \mu^{18}O \\ \mu^2H \\ \varepsilon \end{bmatrix}_{stream\ water} = \sum_{i=1}^N f_i \cdot \begin{bmatrix} \mu^{18}O \\ \mu^2H \\ \varepsilon \end{bmatrix}_{runoff\ component\ i} \\ f \sim Dirichlet(\alpha) \\ \alpha = \rho + \psi \\ [\rho, \psi] \sim Multi_normal(\beta, \Omega) \end{cases} \quad \begin{matrix} (9a) \\ (9b) \\ (9c) \\ (9d) \end{matrix}$$

where, N is the number of runoff components. The contribution vector (f) is represented by a Dirichlet distribution with an index vector α (Eq. 9b), in which the sum of contributions of all runoff components ($\sum f_i$) equals one. The index vector α is estimated by two variable vectors ρ and ψ (Eq. 9c), considering the temporal and spatial variability in the CRC (Cable et al. 2011). ρ and ψ are assumed as bivariate normal distribution with means and precision matrix β and Ω (Eq. 9d). β is a parameter vector estimated by likelihood observations (Table 3).

The value ranges for the parameters need to be estimated in Eqs. 6-9 are summarized in Table 3. The posteriors of parameters describing the spatial variability of tracer signatures in Eqs. 7 and 8b are first estimated by the mean tracer signatures of runoff components measured at different spatial locations. Parameters describing the overall variability of tracer signatures in Eqs. 6 and 8a are then constrained by the likelihood observations of tracer signatures from all water samples at different times and locations. The posterior distribution of CRC (f) are estimated by Eq. 9, based on the posterior tracer signatures of runoff components and the measured tracer signatures from stream water samples. The posteriors of parameters and contributions are estimated by the *R* software package *Rstan*. We run four parallel Markov Chain Monte Carlo (MCMC) chains with 2000 iterations for each chain. The first 1000 iterations are discarded for warm-up, generating a total of 4*1000 samples for the calculation of the posterior distributions. Uncertainties are presented as the 5-95 percentile ranges from the

iterative runs. The parameter values are assumed to follow uniform prior distributions within the value ranges to initialize the MCMC procedure.

To be noted, the four-components approaches (EMMA_4, Bayesian_4_OHcor and Bayesian_4_OHind) are developed in our study to investigate the two following questions: (1) Is the EMMA able to quantify four runoff components just using $\delta^{18}\text{O}$, $\delta^2\text{H}$, and EC? (2) Does the correlation between $\delta^{18}\text{O}$ and $\delta^2\text{H}$ help to reduce the uncertainty in the quantification of runoff components? The correlation between $\delta^{18}\text{O}$ and $\delta^2\text{H}$ is ignored in Bayesian_4_OHind. We used independent prior distributions for $\delta^{18}\text{O}$ and $\delta^2\text{H}$ of each water source. In Bayesian_4_OHcor, the posterior parameters describing the correlation between $\delta^{18}\text{O}$ and $\delta^2\text{H}$ vary among the water sources, thus providing a basis for the quantification of four runoff components using four mixing equations of tracer signatures (similar to Eq.9).

3.3 Effects of the uncertainty in the meltwater sampling

Due to limited accessibility, meltwater samples are typically difficult to collect in high-elevation glacierized areas. Often, only small sample sizes are available to represent the tracer signatures of meltwater generated from the entire glacierized area. Hence, the representativeness of meltwater samples implies an additional uncertainty source in the hydrograph separation

We thus define three virtual sampling scenarios to evaluate the effect of meltwater sampling on the EMMA and Bayesian mixing approaches. Scenario I is used to evaluate the effects of sample size of meltwater, in which four groups of meltwater sample are tested. The four sample groups have the same mean value and *Sd* of $\delta^{18}\text{O}$ or EC, but different sample sizes. Mean and *Sd* values of $\delta^{18}\text{O}$ or EC are calculated for all used meltwater samples in each group, referring to the spatial-temporal variability (same in the two following scenarios). Scenario II is used to evaluate the effects of sampled mean value of $\delta^{18}\text{O}$ (or EC) of meltwater. The four sample groups have the same sample size and *Sd*, but different mean values of $\delta^{18}\text{O}$ (or EC). Scenario III is used to investigate the effects of *Sd* values of sampled $\delta^{18}\text{O}$ (or EC). The four sample groups have the same sample size and mean tracer signature, but different *Sd* values. We investigated the effects of the meltwater sampling uncertainty on the mixing approaches in the glacier melt season, since meltwater is particularly difficult to collect and is the dominant runoff component in this season. For the water samples of other runoff components and stream water, we used all the available measurements in the glacier melt season for the three virtual scenarios, keeping the same sample characteristics. We investigated the effects of sampling uncertainty only in the glacier melt seasons because of the following reasons: (1) Runoff in the glacier melt season contributes the largest part to annual runoff in our study basin. Accurate

quantification of each runoff component in this season is extremely important for the understanding of dynamics of water availability in the study area. Quantifying the uncertainty in the contributions of runoff components caused by sampling uncertainty of meltwater is highly needed in this season; (2) There are more meltwater samples available in this season (15 snowmelt samples and 23 glacier melt samples) than in the snowmelt season (only 15 snowmelt, Table 1), thus providing a good observation data basis for the investigation.

3.4 Effects of water isotope fractionation on hydrograph separation

The water sources for runoff, such as rainfall and meltwater, are subject to evaporation before reaching the basin outlet, especially in summer. However, the isotopic composition of stream water was measured at the basin outlet, and the contributions of runoff components are quantified for the total runoff at the basin outlet. After the long routing path from the sampled sites to the basin outlet, the isotopic compositions of rainfall and meltwater mixing at the basin outlet could be different from those measured at the sampled sites, caused by the evaporation fractionation effect. To consider the changes in the isotope signatures of water sources caused by the fractionation effect during the mixing process, we set up two modified Bayesian approaches, i.e., Bayesian_3_OHcor_Frac and Bayesian_4_OHcor_Frac (Table 2). The fractionation effect on the estimated CRC is quantified by comparing two Bayesian scenarios. In the first scenario (using Bayesian_3_OHcor and Bayesian_4_OHcor), the isotopic compositions of water sources at the basin outlet are assumed the same as those measured from the sample sites even though the water sources have suffered evaporation before reaching the basin outlet (using Eqs. 6-9). In the second scenario (using Bayesian_3_OHcor_Frac and Bayesian_4_OHcor_Frac), the evaporation fractionation effect on the isotopic compositions of water sources is considered, and the mixing of water tracers for stream water is represented by Eq.10. We modify the mean values in Eq. 9a using fractionation factors $\xi^{18}\text{O}$ and $\xi^2\text{H}$. The priors for $\xi^{18}\text{O}$ and $\xi^2\text{H}$ are assumed as bivariate normal distributions in Eq.11.

$$\begin{bmatrix} \mu^{18}\text{O} \\ \mu^2\text{H} \end{bmatrix}_{\text{stream water}} = \sum_{i=1}^N f_i \cdot \begin{bmatrix} \mu^{18}\text{O} + \xi^{18}\text{O} \\ \mu^2\text{H} + \xi^2\text{H} \end{bmatrix}_{\text{runoff component } i} \quad (10)$$

$$\begin{bmatrix} \xi^{18}\text{O} \\ \xi^2\text{H} \end{bmatrix} \sim \text{Multi_normal} \left(\begin{bmatrix} \eta^{18}\text{O} \\ \eta^2\text{H} \end{bmatrix}, \boldsymbol{\Omega} \right) \quad (11)$$

where, $\eta^{18}\text{O}$ and $\eta^2\text{H}$ are parameters describing the mean values of the changes in isotopes caused by the fractionation effect. $\boldsymbol{\Omega}$ is the inverse of the covariance matrix defined in Eq. 6b. The parameters in Eqs. 6-11 are then re-estimated by the measurements of tracer signatures using the MCMC procedure. In particular, parameters describing the prior distributions of

isotopic compositions at the sample sites in Eqs. 6-7 are estimated by the likelihood observations of isotope signatures of runoff components. The fractionation factors $\xi^{18}\text{O}$ and $\xi^2\text{H}$ are estimated by the likelihood observations of isotope signatures of stream water.

4. Results

4.1 Seasonality of tracer signatures

Tracer measurements from all the water samples are summarized in Table 1 and Fig. 2 (see also Fig. S1). The mean values in Table 1 indicate that precipitation is most depleted in heavy water isotopes (^{18}O and ^2H) in the cold season among the water sources. In the melt seasons, snow and glacier meltwater show the most depleted heavy isotopes. The EC values are highest in groundwater in all seasons, followed by stream water and precipitation. Among the water sources, snowmelt and glacier melt tend to have the lowest EC values. Figure 2 shows that the slope of the local meteoric water line (LMWL) is lower than that of the global meteoric water line (GMWL). The $\delta^{18}\text{O}$ of precipitation and snowmelt range from -22.82‰ to 1.51‰ and from -17.31‰ to -6.95‰ , respectively. The isotopic composition of glacier meltwater is more depleted than those of groundwater and stream water. Stream water shows a similar isotopic composition to groundwater. Three samples from the stream water are far below the LMWL, which is likely caused by the evaporation effect.

CV values in Table 1 and boxplots in Figs. 3a-f show that the $\delta^{18}\text{O}$ and $\delta^2\text{H}$ of precipitation generally shows the largest variability in all seasons, followed by the isotopes of snowmelt. Groundwater and stream water show the smallest CV values for $\delta^{18}\text{O}$ in all three seasons. The stream water presents the lowest CV value for EC in all seasons, followed by the groundwater. The snowmelt EC shows high CV values in the snowmelt and glacier melt seasons, which may be attributed to variable dust conditions at the sampling locations (from downstream gauge station to upper glacier accumulation zone). The highest CV value of EC for glacier melt indicates large variability in the glacier melt samples (see also Figs. 3g-i). This is because the glacier melt water samples were collected from a rather clean location (EC value is only $1.5\text{ }\mu\text{S/cm}$) and a relatively dusty location (EC value is $33.4\text{ }\mu\text{S/cm}$).

For each water source except groundwater, the tracer signatures show a significant seasonality (Table 1 and Fig. 3). In particular, the $\delta^{18}\text{O}$ and $\delta^2\text{H}$ of precipitation are most depleted in the cold season and reach the highest values in the glacier melt season, partly caused by the seasonality in temperature. Stream water shows higher values of $\delta^{18}\text{O}$ and EC in the cold season when groundwater dominates the streamflow, and has lower values in the melt seasons when meltwater has a dominant contribution. Snowmelt has a lower EC value in the glacier melt season than in the cold and snowmelt seasons. In the cold and snowmelt seasons, some

snowmelt samples also have EC values as low as those in the glacier melt season. The snow samples in the glacier melt season were only collected from the accumulation zone of the glacier, thus resulting in small variability in the EC values. The snowpack in the accumulation zone is accumulated by fresh snow in the snowy period (summer type accumulation glacier). This leads to low EC values in the snowmelt samples. The tracer signature of groundwater is relatively stable across the seasons.

Figures 3j-l shows the $\delta^{18}\text{O}$ -EC mixing space of runoff components in the three seasons. The ranges of solid lines indicate the minimum and maximum tracer values of individual water samples. In the cold season, the $\delta^{18}\text{O}$ and EC values of stream water are very close to those of groundwater (Fig. 3j), whereas the snowmelt and precipitation tracer signatures show much difference. These results indicate the dominance of groundwater on streamflow during the cold season. In the snowmelt and glacier melt seasons (Figs. 3k-l), the stream water samples are clearly located within the triangle formed by the samples of runoff components. The tracer signatures of glacier meltwater and snowmelt water are similar. The precipitation samples are farther away from the stream water samples compared to the meltwater and groundwater samples. The stream water samples are located nearly in the middle between the meltwater and groundwater samples. This indicates that the contribution of rainfall to total runoff is smallest and the contributions of meltwater and groundwater are similar, in the melt seasons.

4.2 Contributions of runoff components estimated by the mixing approaches

Table 4 and Fig. 4 compare the CRC estimated by the mixing approaches. In the cold season (Fig. 4a), the EMMA_3 estimated the mean contributions of groundwater and snowmelt as 83% and 17%, respectively. The mean contribution of rainfall is zero. The mean contributions of groundwater, snowmelt and rainfall were estimated as 86% (87%), 13% (12%) and 1% (1%) by the Bayesian_3_OHind (Bayesian_3_OHcor) approach. As shown in Fig. 3j, the tracer signature of stream water in this season is close to that of groundwater, while obviously different from that of rainfall. Meanwhile, the stream water samples are outside of the triangle formed by the runoff components, leading to the zero contribution of the rainfall estimated by the EMMA_3.

In the snowmelt season (Fig. 4b and Table 4), the EMMA_3 estimated the mean contributions of groundwater, rainfall and snowmelt as 44%, 36% and 20%, respectively. The Bayesian_3_OHind estimated similar mean CRC to EMMA_3, whereas the Bayesian_3_OHcor delivered a lower contribution of snowmelt (32%). When treating the glacier melt and snowmelt as one end-member (i.e. meltwater) in the glacier melt season (Fig. 4c), the EMMA_3 estimated the mean contributions of groundwater, meltwater and rainfall as

45%, 46% and 9%, respectively. The Bayesian_3_OHind and Bayesian_3_OHcor estimated a lower contribution of groundwater (43-44%) and a higher contribution of rainfall (11%) compared to EMMA_3. The ranges and *Sd* values of CRC in Table 4 indicate the uncertainty in the estimates associated with the corresponding mixing approaches, showing that the EMMA_3 produced the highest uncertainty in CRC in all the three seasons, followed by Bayesian_3_OHind. The Bayesian_3_OHcor slightly reduced the uncertainty compared to Bayesian_3_OHind, benefiting from the consideration of the correlation between $\delta^{18}\text{O}$ and $\delta^2\text{H}$.

When treating glacier melt and snowmelt as two separate end-members in the glacier melt seasons (Fig. 4d), the EMMA_4 failed to separate the hydrograph in the glacier melt season, given the large uncertainty range in the contributions of snowmelt and rainfall (0-100%). The tracer signatures of snow and glacier meltwater are rather close to each other, that violates the second assumption of the EMMA (see Sec. 3.1). In contrast, the Bayesian_4_OHcor and Bayesian_4_OHind estimated the shares of glacier melt and snowmelt as 25-24% and 21-25%, respectively. Considering the significant snow cover area in September in the study basin (He et al. 2018; He et al. 2019), the contribution of snowmelt in the glacier melt season should be higher than zero. Again, the Bayesian_4_OHcor produced smaller uncertainty ranges and *Sd* values for the contributions of groundwater and meltwater compared to Bayesian_4_OHind and EMMA_4 (Table 4).

The posterior distributions of tracer signatures estimated by the Bayesian_4_OHcor in the glacier melt season are compared with the measured histograms of tracer signatures in Fig. 5. The Bayesian_4_OHcor generally produced similar distributions of water isotopes to the measured distributions, in terms of the similar mean values. The estimated posterior *Sd* values of the water isotopes are smaller than *Sd* values of the measurements. This can be explained by the incorporation of prior distributions by the Bayesian_4_OHcor, thus reducing the variability of water isotopes. The posterior *Sd* values for EC of water sources are also smaller than the measured *Sd* values. However, the posterior distributions of EC show some deviations from the distributions of measured EC (Figs. 5k-o), partly due to the very small sample sizes (see Table 1). The comparison between the posterior distributions of tracer signatures estimated by the Bayesian_3_OHcor and the measured distributions in the other seasons generally shows a similar behavior (not shown for brevity).

The Bayesian_4_OHind estimated similar posterior distributions of tracer signatures to the Bayesian_4_OHcor (except the glacier melt isotopes, Fig. 6), with similar mean tracer values and *Sd*. It is noted that the Bayesian_4_OHcor estimated smaller *Sd* values for most water sources than the Bayesian_4_OHind (e.g., Figs. 6f-g and 6i-j). Benefiting from the prior

information and the consideration of the correlation between $\delta^{18}\text{O}$ and $\delta^2\text{H}$, the Bayesian_4_OHcor tended to produce the smallest variability in the posterior tracer signatures among all the mixing approaches (Figs. 5-6), thus resulting in the smallest uncertainty for CRC (Fig. 4d). Figure 7 compares the correlation between $\delta^{18}\text{O}$ and $\delta^2\text{H}$ of the measured tracers and the posterior estimates by Bayesian approaches. The Bayesian_4_OHcor reproduced the correlation between $\delta^{18}\text{O}$ and $\delta^2\text{H}$ well in comparison to the measured data, whereas the Bayesian_4_OHind failed to capture the correlation.

4.3 Uncertainty of hydrograph separation caused by sampling uncertainty of meltwater

Figure 8 shows the sensitivity of the Bayesian_3_OHcor and EMMA_3 approaches to the sampled $\delta^{18}\text{O}$ of meltwater in the glacier melt season. The mean CRC quantified by the two mixing approaches shows minor sensitivity to the sample size (scenario I). However, the uncertainty ranges of contributions tend to decrease with increasing sample size, especially for EMMA_3. When assuming only two meltwater samples, the EMMA_3 resulted in very large uncertainty ranges (0-100%, Fig. 8d), due to the very wide confidence interval for the S_d at a sample size of two. The mean contributions of groundwater and meltwater estimated by the two mixing approaches decrease with increasing mean $\delta^{18}\text{O}$ of the adopted meltwater sample (scenario II), while the estimated contribution of rainfall increases with the increasing mean $\delta^{18}\text{O}$ (Fig. 8k). Variations in the mean CRC quantified by EMMA_3 are larger than those estimated by the Bayesian_3_OHcor. Using EMMA_3, both the mean contributions of groundwater and meltwater declined by 9% with the assumed increase of the mean $\delta^{18}\text{O}$ (Figs. 8e and 8h), and the contribution of rainfall increased by 17%. Using Bayesian_3_OHcor, the reduction of contributions of groundwater and snowmelt are 4% and 7%, respectively, and the increase of contribution of rainfall is only 11% (Fig. 8k). In scenario III, the uncertainty ranges of CRC (especially for rainfall, Fig. 8l) increase with increasing S_d of the sampled $\delta^{18}\text{O}$. Again, the increases in the uncertainty ranges estimated by EMMA_3 tend to be larger than those estimated by the Bayesian_3_OHcor. The sensitivity of the mixing approaches to the sampled EC values of the meltwater are similar to the sensitivity to the sampled $\delta^{18}\text{O}$ (not shown).

4.4 Effect of isotope fractionation on the hydrograph separation

The changes of $\delta^{18}\text{O}$ caused by the fractionation effect (referring to $\xi^{18}\text{O}$ in Eq. 10) during the mixing process are estimated in Figs. 9a-c. The fractionation has the smallest effect on the $\delta^{18}\text{O}$ of groundwater, while the largest effect on the $\delta^{18}\text{O}$ of rainfall. On average, the $\delta^{18}\text{O}$ of rainfall increased by around 2.8‰ through fractionation in all the three seasons. The CRC estimated by the Bayesian_3_OHcor_Frac and Bayesian_4_OHcor_Frac are compared with those estimated by the Bayesian_3_OHcor and Bayesian_4_OHcor in Figs. 9d-f,

respectively. The mean contribution of groundwater estimated by the Bayesian_3_OHcor_Frac in the cold season is 9% lower than that estimated by the Bayesian_3_OHcor (Fig. 9d), while the mean contributions of snowmelt and rainfall are 3% and 5% higher, respectively. The reduction of groundwater contribution is compensated by the increased contributions of snowmelt and rainfall caused by the fractionation effect. In the snowmelt season, the mean contributions of groundwater and rainfall are 1% and 7% lower (Fig. 9e), while the mean contribution of snowmelt estimated by the Bayesian_3_OHcor_Frac is 8% higher. In the glacier melt season, the mean contributions of groundwater and meltwater estimated by the Bayesian_4_OHcor_Frac are higher than those estimated by the Bayesian_4_OHcor (Fig. 9f), and are compensated by the 6% lower contribution of rainfall.

The fractionation effect also produced visible changes on the posterior distributions of $\delta^{18}\text{O}$ and $\delta^2\text{H}$ of runoff components (Fig. 10 shows the example in the glacier melt season). The mean isotopic compositions of runoff components are increased by the fractionation effect. The *Sd* values of the posterior isotopes estimated by the Bayesian_4_OHcor_Frac tend to be higher than those estimated by the Bayesian_4_OHcor, due to the increased parameter space in the prior assumptions (Eq. 11), thus leading to the larger uncertainty ranges in the contributions of glacier melt and snowmelt (Fig. 9f). As expected, the estimates of posterior distributions of isotopic compositions of stream water are less sensitive to the fractionation effect of runoff components (Figs. 10e and 10j). The fractionation also has minor effects on the estimates of posterior distributions of EC values (Figs. 10k-o).

5. Discussion

5.1 Uncertainty of the contributions of runoff components

The EMMA estimated similar CRCs but with a larger uncertainty than the Bayesian approaches. The reasons for this are two-fold. First, the EMMA estimated the uncertainty ranges of CRC using the standard deviations (*Sd*) of the measured tracer signatures. *Sd* values are likely overestimated in this study due to the small sample sizes, and thus insufficiently representing the variability of the tracer signatures of the corresponding water sources across the basin. Due to the limited accessibility of the sample sites caused by snow cover, the water samples of meltwater and groundwater are often collected sporadically. The small sample size and strong variability in sampled tracer signatures likely led to a large *Sd* value. Second, the EMMA assumes that the uncertainty associated with each water source is independent from the uncertainty of other water sources (Eq.5), which increases the uncertainty ranges for CRC.

In contrast, the Bayesian approaches estimated smaller variability of tracer signatures in the posterior distributions compared to the measured tracer signatures, by updating the prior

probability distributions. The posterior distributions were sampled continuously from the assumed value ranges by the MCMC runs, thus reducing the sharp changes and yielding lower variability for the tracer signatures. Moreover, the uncertainty ranges for CRC were quantified using Eqs. 6-10, instead of calculating independently as in the EMMA. Additionally, the assumed prior distributions of tracer signatures and the CRC take into account the correlation between the tracer signatures and the dependence between the runoff components in the Bayesian approaches, thus resulting in smaller uncertainty ranges (Soulsby et al., 2003). For example, the Bayesian approaches considering the correlation between $\delta^{18}\text{O}$ and $\delta^2\text{H}$ generally estimated smaller uncertainty ranges for CRC compared to those without considering this correlation.

The Gaussian error propagation technique is only capable of considering the uncertainty of CRC resulting from the variation in the tracer signatures (Uhlenbrook and Hoeg, 2003). The uncertainty of CRC originated from the sampling uncertainty of meltwater was then investigated in separate virtual sampling experiments. The EMMA produces large uncertainty ranges and *Sd* values for CRC in the glacier melt season, when the meltwater sample size is rather small. The mean CRC quantified by the EMMA relies more heavily on the mean tracer values of the sampled meltwater, as the mean tracer values are directly used in Eqs. 1-4, in comparison to the mean CRC estimated by the Bayesian approach.

The EMMA assumes that the tracer signature of each runoff component is constant during the mixing process, thus is unable to estimate the uncertainty of CRC caused by the isotope fractionation effect. The virtual fractionation experiments using the modified Bayesian approaches show that the isotope fractionation could increase the contribution of snowmelt by 8%, and reduce the contribution of rainfall by 7% in the snowmelt season. We assume the mean CRC estimated by the Bayesian approaches considering the isotope fractionation are more plausible, despite the larger uncertainty ranges. Along the flow path from the source areas to the river channel, the isotopic compositions of meltwater and rainfall are likely increased by the evaporation fractionation effect, especially in the warm seasons. The increased isotopic compositions of meltwater and rainfall during the routing process need to be considered in the mixing approaches for hydrograph separation.

In general, the uncertainty of CRC is visibly caused by the spatio-temporal variability in the tracer signatures, the water sampling uncertainty and the isotope fractionation during the mixing process. The uncertainty caused by the water sampling of meltwater tends to be smaller than the uncertainty caused by the variations of the tracer signatures in both the EMMA and Bayesian mixing approaches. This is consistent to the findings that the *Sd* values of the tracer

measurements of water samples are the main uncertainty sources for the quantification of CRC (Schmieder et al., 2016; Schmieder et al., 2018). The Bayesian approach tends to be superior on narrowing the variability of posterior tracer signatures benefiting from the prior assumptions and the consideration of the dependence between tracer signatures and runoff components compared to EMMA.

5.2 Limitations

The representativeness of the water samples is one of the limitations of this study. The groundwater was only sampled from a single spring located at the elevation of 2400 m a.s.l., which is rather close to the average altitude of the entire river network in the study basin (2530 m a.s.l.). We thus assume that the measured isotopic composition of the spring water represents the mean isotopic composition of groundwater feeding the river in the basin (see also He et al., 2019). Collecting samples from a few springs to represent the groundwater end-member has been proposed before (such as Ohlanders et al., 2013 and Mark and McKenzie, 2007), as the accessibility and availability of more potential springs are hampered. Again, for the snow and glacier meltwater samples, we assume that meltwater occurring at similar elevations have similar tracer signatures (He et al., 2019). The sampled elevation ranges from 1580 m to 4050 m a.s.l., matching with the elevation range where meltwater mainly occurs in the basin (from 1580 m to 3950 m a.s.l.). Considering the isotopic compositions of meltwater are particularly dependent on the elevation, the sampled meltwater could represent meltwater originated from the primary melting locations in the entire basin. The sampled sites thus bear the potential to provide tracer signatures of the major meltwater generated in the basin. We split the entire sampling period (years of 2012 to 2017) into three seasons, i.e. cold season, snowmelt season and glacier melt season, due to the low availability of water samples in each year. By concentrating water samples in the three seasons, we increased the sample sizes of each runoff component for each season, thus increasing the ability of water samples to represent the spatio-temporal variability of seasonal tracer signatures. We used all available groundwater and snowmelt samples from the three seasons for hydrograph separation in the cold season, due to the rather low sample sizes collected in the cold season. This likely leads to overestimated contributions of groundwater and snowmelt in the cold season. However, the overestimation of groundwater contribution is probably small because the tracer signatures of groundwater generally show small seasonal variability. The estimated contributions of snowmelt in the cold season are a bit higher than the contribution modeled by He et al (2018) during DJF (December, January and February), but are still reasonable considering the cold season includes October and November when snow is more prone to melt than DJF.

The assumptions of the mixing approaches lead to another limitation of this study. The EMMA assumes the tracer signatures of water sources are constant during the mixing process, which is a common assumption for the practical application of EMMA. It thus fails to consider the uncertainty originating from the changes of tracer signatures. In the Bayesian approach, we assumed normal prior distributions for the tracer signatures of water sources and Dirichlet prior distribution for the CRC based on literature knowledge (Cable et al., 2011). To refine the description of the temporal and spatial variability of the CRC in the Dirichlet distribution, more hydrological data relating to the runoff processes in the basin are required. We acknowledge that the estimated CRC could be strongly affected by the assumptions of prior distributions. However, testing the effects of the prior assumptions goes beyond the scope of this study. We assume that collecting more water samples from various locations and at different time for each water source could improve the estimation of tracer signature distributions.

6. Conclusions

This study compared the Bayesian end-member mixing approach with a traditional end-member mixing approach (EMMA) for hydrograph separation in a glacierized basin. The contributions of runoff components (CRC) to the total runoff were estimated for three seasons, i.e. cold season, snowmelt and glacier melt seasons. Uncertainty of these contributions caused by the variability of tracer signatures, water sampling uncertainty and isotope fractionation were evaluated as follows.

(1) The Bayesian approach generally estimates smaller uncertainty ranges of CRC, in comparison to the EMMA. Benefiting from the prior assumptions on tracer signatures and CRC, as well as from the incorporation of the correlation between tracer signatures in the prior distributions, the Bayesian approach reduced the uncertainty. The Bayesian approach jointly quantified the uncertainty ranges of CRC. In contrast, the EMMA estimated the uncertainty of contribution of each runoff component independently, thus leading to higher uncertainty ranges.

(2) The estimates of CRC in EMMA tend to be more sensitive to the sampling uncertainty of meltwater, compared to those in the Bayesian approach. For small sample sizes (e.g., two), EMMA estimated very large uncertainty ranges. The mean CRC quantified by EMMA are also more sensitive to the mean value of the tracer signature of the meltwater samples than those estimated by the Bayesian approach are.

(3) Ignoring the isotope fractionation during the mixing process likely overestimates the contribution of rainfall and underestimates the contribution of meltwater in the melt seasons. The currently used EMMA is unable to quantify the uncertainty of CRC caused by the isotope fractionation during the mixing process, due to the underlying assumptions.

Code availability: The R code for the Bayesian end-member mixing approach can be found at https://www.dropbox.com/s/kf2xy3s4vt718s9/Bayesian%20mixing%20approach_four%20components.stan?dl=0

Author contributions.

Conceptualization: Zhihua He, Katy Unger-Shayesteh, and Sergiy Vorogushyn; Data collection: Zhihua He, Katy Unger-Shayesteh, Stephan M. Weise, Olga Kalashnikova, and Abror Gafurov; Methodology: Zhihua He, Katy Unger-Shayesteh, and Sergiy Vorogushyn; Writing original draft: Zhihua He, Sergiy Vorogushyn, and Doris Duethmann; Writing review and editing, All

Competing interests.

The authors declare no conflict of interest.

Acknowledgement

Our work has been funded by the German Federal Ministry for Science and Education (project GlaSCA-V, grant number 88 501) and Volkswagen Foundation (project GlaSCA, grant number 01DK15002A and B), respectively.

Reference

- Aizen, V., Aizen, E., Glazirin, G., and Loaiciga, H. A.: Simulation of daily runoff in Central Asian alpine watersheds, *Journal of Hydrology*, 238, 15-34, [https://doi.org/10.1016/S0022-1694\(00\)00319-X](https://doi.org/10.1016/S0022-1694(00)00319-X), 2000.
- Aizen, V. B., Aizen, E. M., and Melack, J. M.: Precipitation, melt and runoff in the northern Tien Shan, *Journal of Hydrology*, 186, 229-251, [https://doi.org/10.1016/S0022-1694\(96\)03022-3](https://doi.org/10.1016/S0022-1694(96)03022-3), 1996.
- Aizen, V. B., Kuzmichenok, V. A., Surazakov, A. B., and Aizen, E. M.: Glacier changes in the Tien Shan as determined from topographic and remotely sensed data, *Global and Planetary Change*, 56, 328-340, <https://doi.org/10.1016/j.gloplacha.2006.07.016>, 2007.
- Barnett, T. P., Adam, J. C., and Lettenmaier, D. P.: Potential impacts of a warming climate on water availability in snow-dominated regions, *Nature*, 438, 303–309, doi:10.1038/nature04141, 2005.
- Beria, H., Larsen, J. R., Michelon, A., Ceperley, N. C., and Schaefli, B.: HydroMix v1.0: a new Bayesian mixing framework for attributing uncertain hydrological sources, *Geoscientific Model Development Discussion*, <https://doi.org/10.5194/gmd-2019-69>, in review, 2019.
- Brown, L. E., Hannah, D. M., Milner, A. M., Soulsby, C., Hodson, A. J., and Brewer, M. J.: Water source dynamics in a glacierized alpine river basin (Taillon-Gabietous, French Pyrenees), *Water Resources Research*, 42, W08404, doi:10.1029/2005WR004268, 2006.
- Cable, J., Ogle, K., and Williams, D.: Contribution of glacier meltwater to streamflow in the Wind River Range, Wyoming, inferred via a Bayesian mixing model applied to isotopic measurements, *Hydrological Processes*, 25, 2228-2236, doi:10.1002/hyp.7982, 2011.
- Chiogna, G., Santoni, E., Camin, F., Tonon, A., Majone, B., Trenti, A., and Bellin, A.: Stable isotope characterization of the Vermigliana catchment, *Journal of Hydrology*, 509, 295-305, <https://doi.org/10.1016/j.jhydrol.2013.11.052>, 2014.
- Dahlke, H. E., Lyon, S. W., Jansson, P., Karlin, T., and Rosqvist, G.: Isotopic investigation of runoff generation in a glacierized catchment in northern Sweden, *Hydrological Processes*, 28, 1383-1398, doi:10.1002/hyp.9668, 2014.
- Engel, M., Penna, D., Bertoldi, G., Dell'Agnese, A., Soulsby, C., and Comiti, F.: Identifying run-off contributions during melt-induced run-off events in a glacierized alpine catchment, *Hydrological Processes*, 30, 343-364, doi:10.1002/hyp.10577, 2016.

- Genereux, D.: Quantifying uncertainty in tracer-based hydrograph separations, *Water Resources Research*, 34, 915-919, <https://doi.org/10.1029/98WR00010>, 1998.
- Gröning, M., Lutz, H.O., Roller-Lutz, Z., Kralik, M., Gourcy, L., and Pöltenstein, L.: A simple rain collector preventing water reevaporation dedicated for $\delta^{18}\text{O}$ and $\delta^2\text{H}$ analysis of cumulative precipitation samples, *Journal of Hydrology*, 448–449, 195–200, doi: 10.1016/j.jhydrol.2012.04.041, 2012.
- He, Z. H., Parajka, J., Tian, F. Q., and Blöschl, G.: Estimating degree-day factors from MODIS for snowmelt runoff modeling, *Hydrology and Earth System Sciences*, 18, 4773–4789, <https://doi.org/10.5194/hess-18-4773-2014>, 2014.
- He, Z. H., Tian, F. Q., Gupta, H. V., Hu, H. C., and Hu, H. P.: Diagnostic calibration of a hydrological model in a mountain area by hydrograph partitioning, *Hydrology and Earth System Sciences*, 19, 1807–1826, <https://doi.org/10.5194/hess-19-1807-2015>, 2015.
- He, Z., Unger-Shayesteh, K., Vorogushyn, S., Weise, S. M., Kalashnikova, O., Gafurov, A., Duethmann, D., Barandun, M., and Merz, B.: Constraining hydrological model parameters using water isotopic compositions in a glacierized basin, Central Asia, *Journal of Hydrology*, 571, 332–348, <https://doi.org/10.1016/j.jhydrol.2019.01.048>, 2019.
- He, Z., Vorogushyn, S., Unger-Shayesteh, K., Gafurov, A., Kalashnikova, O., Omorova, E., and Merz, B.: The Value of Hydrograph Partitioning Curves for Calibrating Hydrological Models in Glacierized Basins, *Water Resources Research*, 54, 2336–2361, doi.org/10.1002/2017WR021966, 2018.
- Joerin, C., Beven, K. J., Iorgulescu, I., and Musy, A.: Uncertainty in hydrograph separations based on geochemical mixing models, *Journal of Hydrology*, 255, 90–106, [https://doi.org/10.1016/S0022-1694\(01\)00509-1](https://doi.org/10.1016/S0022-1694(01)00509-1), 2002.
- Klaus, J., and McDonnell, J. J.: Hydrograph separation using stable isotopes: Review and evaluation, *Journal of Hydrology*, 505, 47–64, <https://doi.org/10.1016/j.jhydrol.2013.09.006>, 2013.
- Kong, Y. L., and Pang, Z. H.: Evaluating the sensitivity of glacier rivers to climate change based on hydrograph separation of discharge, *Journal of Hydrology*, 434, 121–129, <https://doi.org/10.1016/j.jhydrol.2012.02.029>, 2012.
- La Frenierre, J., and Mark, B. G.: A review of methods for estimating the contribution of glacial meltwater to total watershed discharge, *Progress in Physical Geography*, 38, 173–200, doi:10.1177/0309133313516161, 2014.

- Li, Z. X., Feng, Q., Liu, W., Wang, T. T., Cheng, A. F., Gao, Y., Guo, X. Y., Pan, Y. H., Li, J. G., Guo, R., and Jia, B.: Study on the contribution of cryosphere to runoff in the cold alpine basin: A case study of Hulugou River Basin in the Qilian Mountains, *Global and Planetary Change*, 122, 345-361, <https://doi.org/10.1016/j.gloplacha.2014.10.001>, 2014.
- Mark, B. G., and Mckenzie, J. M.: Tracing increasing tropical Andean glacier melt with stable isotopes in water, *Environmental Science & Technology*, 41, 6955-6960, <https://doi.org/10.1021/es071099d>, 2007.
- Maurya, A. S., Shah, M., Deshpande, R. D., Bhardwaj, R. M., Prasad, A., and Gupta, S. K.: Hydrograph separation and precipitation source identification using stable water isotopes and conductivity: River Ganga at Himalayan foothills, *Hydrological Processes*, 25, 1521-1530, doi:10.1002/hyp.7912, 2011.
- Moore, J. W., and Semmens, B. X.: Incorporating uncertainty and prior information into stable isotope mixing models, *Ecology Letters*, 11, 470-480, doi:10.1111/j.1461-0248.2008.01163.x, 2008.
- Ohlanders, N., Rodriguez, M., and McPhee, J.: Stable water isotope variation in a Central Andean watershed dominated by glacier and snowmelt, *Hydrology and Earth System Sciences*, 17, 1035-1050, doi:10.5194/hess-17-1035-2013, 2013.
- Parnell, A. C., Inger, R., Bearhop, S., and Jackson, A. L.: Source Partitioning Using Stable Isotopes: Coping with Too Much Variation, *PLoS ONE* 5(3): e9672. doi:10.1371/journal.pone.0009672, doi:10.1371/journal.pone.0009672, 2010.
- Penna, D., Engel, M., Bertoldi, G., and Comiti, F.: Towards a tracer-based conceptualization of meltwater dynamics and streamflow response in a glacierized catchment, *Hydrology and Earth System Sciences*, 21, 23-41, doi:10.5194/hess-21-23-2017, 2017.
- Penna, D., Engel, M., Mao, L., Dell'Agnese, A., Bertoldi, G., and Comiti, F.: Tracer-based analysis of spatial and temporal variations of water sources in a glacierized catchment, *Hydrology and Earth System Sciences*, 18, 5271-5288, doi:10.5194/hess-18-5271-2014, 2014.
- Penna, D., van Meerveld, H. J., Zuecco, G., Fontana, G. D., and Borga, M.: Hydrological response of an Alpine catchment to rainfall and snowmelt events, *Journal of Hydrology*, 537, 382-397, <https://doi.org/10.1016/j.jhydrol.2016.03.040>, 2016.
- Pohl, E., Gloaguen, R., Andermann, C., and Knoche, M.: Glacier melt buffers river runoff in the Pamir Mountains, *Water Resources Research*, 53, 2467-2489, doi:10.1002/2016WR019431, 2017.

- Pu, T., He, Y. Q., Zhu, G. F., Zhang, N. N., Du, J. K., and Wang, C. F.: Characteristics of water stable isotopes and hydrograph separation in Baishui catchment during the wet season in Mt. Yulong region, south western China, *Hydrological Processes*, 27, 3641-3648, doi:10.1002/hyp.9479, 2013.
- Pu, T., Qin, D. H., Kang, S. C., Niu, H. W., He, Y. Q., and Wang, S. J.: Water isotopes and hydrograph separation in different glacial catchments in the southeast margin of the Tibetan Plateau, *Hydrological Processes*, 31, 3810-3826, doi:10.1002/hyp.11293, 2017.
- Rahman, K., Besacier-Monbertrand, A. L., Castella, E., Lods-Crozet, B., Ilg, C., and Beguin, O.: Quantification of the daily dynamics of streamflow components in a small alpine watershed in Switzerland using end member mixing analysis, *Environmental Earth Sciences*, 74, 4927-4937, <https://doi.org/10.1007/s12665-015-4505-5>, 2015.
- Schmieder, J., Garvelmann, J., Marke, T., and Strasser, U.: Spatio-temporal tracer variability in the glacier melt end-member How does it affect hydrograph separation results, *Hydrological Processes*, 32, 1828-1843, doi:10.1002/hyp.11628, 2018.
- Schmieder, J., Hanzer, F., Marke, T., Garvelmann, J., Warscher, M., Kunstmann, H., and Strasser, U.: The importance of snowmelt spatiotemporal variability for isotope-based hydrograph separation in a high-elevation catchment, *Hydrology and Earth System Sciences*, 20, 5015-5033, doi:10.5194/hess-20-5015-2016, 2016.
- Soulsby, C., Petry, J., Brewer, M. J., Dunn, S. M., Ott, B., and Malcolm, I. A.: Identifying and assessing uncertainty in hydrological pathways: a novel approach to end member mixing in a Scottish agricultural catchment, *Journal of Hydrology*, 274, 109-128, [https://doi.org/10.1016/S0022-1694\(02\)00398-0](https://doi.org/10.1016/S0022-1694(02)00398-0), 2003.
- Sun, C. J., Chen, Y. N., Li, W. H., Li, X. G., and Yang, Y. H.: Isotopic time series partitioning of streamflow components under regional climate change in the Urumqi River, northwest China, *Hydrological Sciences Journal-Journal Des Sciences Hydrologiques*, 61, 1443-1459, doi:10.1080/02626667.2015.1031757, 2016a.
- Sun, C. J., Yang, J., Chen, Y. N., Li, X. G., Yang, Y. H., and Zhang, Y. Q.: Comparative study of streamflow components in two inland rivers in the Tianshan Mountains, Northwest China, *Environmental Earth Sciences*, 75:727. doi:10.1007/s12665-016-5314-1, 2016b.
- Uhlenbrook, S., and Hoeg, S.: Quantifying uncertainties in tracer-based hydrograph separations: a case study for two-, three- and five-component hydrograph separations in a mountainous catchment, *Hydrological Processes*, 17, 431-453, doi:10.1002/hyp.1134, 2003.

821 Viviroli, D., Durr, H. H., Messerli, B., Meybeck, M., and Weingartner, R.: Mountains of the
822 world, water towers for humanity: Typology, mapping, and global significance, *Water*
823 *Resources Research*, 43, W07447, <https://doi.org/10.1029/2006wr005653>, 2007.

824 Ward, E. J., Semmens, B. X., and Schindler, D. E.: Including Source Uncertainty and Prior
825 Information in the Analysis of Stable Isotope Mixing Models, *Environmental Science*
826 *& Technology*, 44, 4645-4650, doi:10.1021/es100053v, 2010.

827	LIST OF TABLES	
828	Table 1. Tracer signatures measured from water samples in three seasons	29
829	Table 2. Mixing approaches used for hydrograph separation in different seasons	32
830	Table 3. Parameters used for prior distributions in the Bayesian approaches.....	33
831	Table 4. Contributions of runoff components estimated by the different mixing approaches	
832	(%).....	34

833 Table 1. Tracer signatures measured from water samples in three seasons. CV stands for
834 coefficient of variation.

Season	Water source	Tracer	Sample size	Mean	Range	CV
Cold season (October to February)	Groundwater	^{18}O (‰)	23	-11.37	(-12.12, -10.61)	0.04
		^2H (‰)	23	-73.90	(-77.90, -68.20)	0.03
		EC(μs/cm)	13	126.80	(69.60, 167.20)	0.24
	Precipitation	^{18}O (‰)	37	-15.93	(-22.82, -7.70)	0.21
		^2H (‰)	37	-111.50	(-168.80, -39.10)	0.27
		EC(μs/cm)	23	67.80	(21.30, 99.60)	0.34
	Snowmelt	^{18}O (‰)	36	-12.51	(-17.31, -6.95)	0.19
		^2H (‰)	36	-84.60	(-120.70, -38.70)	0.23
		EC(μs/cm)	15	53.70	(8.80, 151.00)	0.96
	Stream water	^{18}O (‰)	150	-11.33	(-11.82, -9.05)	0.03
		^2H (‰)	150	-74.20	(-77.50, -68.20)	0.03
		EC(μs/cm)	90	112.20	(80.30, 139.30)	0.13

835

836 Table 1 Continued.

Season	Water source	Tracer	Sample size	Mean	Range	CV
Snowmelt season (March to June)	Groundwater	^{18}O (‰)	9	-11.34	(-11.94, -11.06)	0.02
		^2H (‰)	9	-73.90	(-77.30, -72.40)	0.02
		EC(μs/cm)	8	133.10	(94.00, 167.20)	0.21
	Precipitation	^{18}O (‰)	25	-7.89	(-16.81, -0.06)	0.46
		^2H (‰)	25	-49.20	(-120.50, -3.90)	0.52
		EC(μs/cm)	11	58.30	(25.80, 84.30)	0.34
	Snowmelt	^{18}O (‰)	15	-13.87	(-16.74, -10.96)	0.11
		^2H (‰)	15	-95.90	(-119.30, -70.50)	0.13
		EC(μs/cm)	11	67.30	(11.00, 151.00)	0.80
	Stream water	^{18}O (‰)	126	-11.58	(-12.91, -10.04)	0.04
		^2H (‰)	126	-76.10	(-86.40, -67.00)	0.04
		EC(μs/cm)	23	94.90	(80.10, 114.00)	0.09

837

838

839 Table 1 Continued.

Season	Water source	Tracer	Sample size	Mean	Range	CV
Glacier melt season (July to September)	Groundwater	^{18}O (‰)	14	-11.40	(-12.12, -10.61)	0.04
		^2H (‰)	14	-73.90	(-77.90, -68.20)	0.04
		EC(μs/cm)	5	116.70	(69.60, 142.60)	0.30
	Precipitation	^{18}O (‰)	28	-6.72	(-13.02, 1.51)	0.56
		^2H (‰)	28	-42.60	(-94.90, 3.00)	0.58
		EC(μs/cm)	9	67.70	(26.70, 102.00)	0.39
	Snowmelt	^{18}O (‰)	15	-12.70	(-17.31, -9.85)	0.15
		^2H (‰)	15	-85.60	(-120.70, -64.00)	0.17
		EC(μs/cm)	4	16.20	(8.80, 24.30)	0.51
	Glacier melt	^{18}O (‰)	23	-13.11	(-14.96, -11.55)	0.10
		^2H (‰)	23	-87.20	(-100.40, -75.50)	0.11
		EC(μs/cm)	10	9.90	(1.50, 33.40)	1.28
	Stream water	^{18}O (‰)	119	-11.75	(-12.97, -5.64)	0.07
		^2H (‰)	119	-77.20	(-86.70, -62.30)	0.05
		EC(μs/cm)	24	64.50	(33.40, 99.30)	0.25

840

841 Table 2. Mixing approaches used for hydrograph separation in different seasons.

Mixing approach	Description	End-member	Used tracers	Seasons applied to
EMMA_3	Three-component traditional end-member mixing approach	Groundwater, snowmelt (or meltwater) and rainfall	^{18}O and EC	Cold season, snowmelt season and glacier melt season
EMMA_4	Four-component traditional end-member mixing approach	Groundwater, snowmelt, glacier melt and rainfall	^{18}O , ^2H and EC	Glacier melt season
Bayesian_3_OHind	Three-component Bayesian approach, without considering the correlation between $\delta^{18}\text{O}$ and $\delta^2\text{H}$	Groundwater, snowmelt (or meltwater) and rainfall	^{18}O and EC	Cold season, snowmelt season and glacier melt season
Bayesian_3_OHcor	Three-component Bayesian approach, considering the correlation between $\delta^{18}\text{O}$ and $\delta^2\text{H}$	Groundwater, snowmelt (or meltwater) and rainfall	^{18}O , ^2H and EC	Cold season, snowmelt season and glacier melt season
Bayesian_3_OHcor_Frac	Three-component Bayesian approach, considering the correlation between $\delta^{18}\text{O}$ and $\delta^2\text{H}$ and the fractionation of $\delta^{18}\text{O}$ and $\delta^2\text{H}$ during the mixing process	Groundwater, snowmelt and rainfall	^{18}O , ^2H and EC	Cold season and snowmelt season
Bayesian_4_OHind	Four-component Bayesian approach, without considering the correlation between ^{18}O and ^2H	Groundwater, snowmelt, glacier melt and rainfall	^{18}O , ^2H and EC	Glacier melt season
Bayesian_4_OHcor	Four-component Bayesian approach, considering the correlation between $\delta^{18}\text{O}$ and $\delta^2\text{H}$	Groundwater, snowmelt, glacier melt and rainfall	^{18}O , ^2H and EC	Glacier melt season
Bayesian_4_OHcor_Frac	Four-component Bayesian approach, considering the correlation between $\delta^{18}\text{O}$ and $\delta^2\text{H}$ and the fractionation of $\delta^{18}\text{O}$ and $\delta^2\text{H}$ during the mixing process	Groundwater, snowmelt, glacier melt and rainfall	^{18}O , ^2H and EC	Glacier melt season

Table 3. Parameters used for prior distributions in the Bayesian approaches.

Parameter	Description	Applied Bayesian approach	Value range	Equation
$\gamma^{18}\text{O}$	Mean of the prior normal distributions for the mean $\delta^{18}\text{O}$ of runoff components	All Bayesian approaches	(-50,50)	Eq.7a
$\gamma^2\text{H}$	Mean of the prior normal distributions for the mean $\delta^2\text{H}$ of runoff components	All Bayesian approaches, except Bayesian_3_OHind	(-200,200)	Eq.7b
$\sigma^{18}\text{O}$	Variance of the prior normal distributions for the mean $\delta^{18}\text{O}$ of runoff components	All Bayesian approaches	(0,50)	Eq.7a
$\sigma^2\text{H}$	Variance of the prior normal distributions for the mean $\delta^2\text{H}$ of runoff components	All Bayesian approaches, except Bayesian_3_OHind	(0,200)	Eq.7b
$\lambda^{18}\text{O}$	Variance of the prior normal distributions for the $\delta^{18}\text{O}$ of runoff components and stream water	Bayesian_3_OHind and Bayesian_4_OHind	(0,50)	Eq.6c
$\lambda^2\text{H}$	Variance of the prior normal distributions for the $\delta^2\text{H}$ of runoff components and stream water	Bayesian_4_OHind	(0,200)	Eq.6d
τ	Variance of the prior normal distributions for the EC of runoff components and stream water	All Bayesian approaches	(0,400)	Eq.8a
θ	Mean of the prior normal distributions for the mean EC of runoff components	All Bayesian approaches	(0,400)	Eq.8b
ω	Variance of the prior normal distributions for the mean EC of runoff components	All Bayesian approaches	(0,400)	Eq.8b
β	Mean of the prior bivariate normal distributions for parameters describing the α value in the Dirichlet distribution of contributions of runoff components	All Bayesian approaches	(0,10)	Eq.9d
$\eta^{18}\text{O}$	Mean of the prior bivariate normal distributions for the fractionations of $\delta^{18}\text{O}$ of runoff components	Bayesian_3_OHcor_Frac and Bayesian_4_OHcor_Frac	(0,5)	Eq.11
$\eta^2\text{H}$	Mean of the prior bivariate normal distributions for the fractionations of $\delta^2\text{H}$ of runoff components	Bayesian_3_OHcor_Frac and Bayesian_4_OHcor_Frac	(0,5)	Eq.11

845 Table 4. Contributions of runoff components (CRC) estimated by the different mixing
846 approaches (percentage, %). The ranges (%) show the difference between the 95% and 5%
847 percentiles. *Sd* values refer to the standard deviations.

	Mixing approach	Groundwater			Snowmelt			Rainfall			Glacier melt			Meltwater		
		Mean	Range	<i>Sd</i>	Mean	Range	<i>Sd</i>	Mean	Range	<i>Sd</i>	Mean	Range	<i>Sd</i>	Mean	Range	<i>Sd</i>
Cold season	EMMA_3	83	41	0.12	17	46	0.17	0	10	0.12	-	-	-	-	-	-
	Bayesian_3_OHind	86	28	0.01	13	28	0.09	1	3	0.09	-	-	-	-	-	-
	Bayesian_3_OHcor	87	24	0.01	12	24	0.07	1	3	0.07	-	-	-	-	-	-
Snowmelt season	EMMA_3	44	50	0.15	36	33	0.11	20	25	0.09	-	-	-	-	-	-
	Bayesian_3_OHind	42	33	0.12	36	22	0.10	22	20	0.07	-	-	-	-	-	-
	Bayesian_3_OHcor	46	30	0.12	32	20	0.09	22	19	0.06	-	-	-	-	-	-
Glacier melt season (three-component)	EMMA_3	45	48	0.13	-	-	-	9	17	0.06	-	-	-	46	35	0.10
	Bayesian_3_OHind	43	25	0.11	-	-	-	11	13	0.06	-	-	-	46	18	0.08
	Bayesian_3_OHcor	44	24	0.11	-	-	-	11	12	0.05	-	-	-	45	17	0.07
Glacier melt season (four-component)	EMMA_4	45	48	0.14	0	100	0.33	11	100	0.35	44	78	0.20	-	-	-
	Bayesian_4_OHind	44	30	0.10	21	42	0.09	10	13	0.13	25	41	0.04	-	-	-
	Bayesian_4_OHcor	41	23	0.10	25	33	0.07	10	13	0.10	24	33	0.04	-	-	-

848

LIST OF FIGURES

Fig. 1. Study area of the Ala-Archa basin and Golubin Glacier including the locations of the water sampling points.....	36
Fig. 2. Isotope signatures of water samples from the three seasons in the Ala-Archa basin	37
Fig. 3. $\delta^{18}\text{O}$ -EC mixing space of the various water sources in the three seasons.....	38
Fig. 4. Contributions of runoff components to total runoff estimated by different mixing approaches in three seasons.....	39
Fig. 5. Posterior distributions of tracer signatures estimated by the Bayesian_4_OHcor.....	40
Fig. 6. Comparison of the posterior distributions of tracer signatures estimated by two Bayesian approaches	41
Fig. 7. Correlation between posterior $\delta^{18}\text{O}$ and $\delta^2\text{H}$ estimated by the Bayesian_4_OHcor and the Bayesian_4_OHind approaches	42
Fig. 8. Sensitivity of the estimates for the contributions of runoff components to the sampling uncertainty.....	43
Fig. 9. Effects of isotope fractionation on the contributions of runoff components in the Bayesian approaches.....	44
Fig. 10. Effects of isotope fractionation on the posterior distributions of tracer signatures of water sources in the glacier melt season.....	45

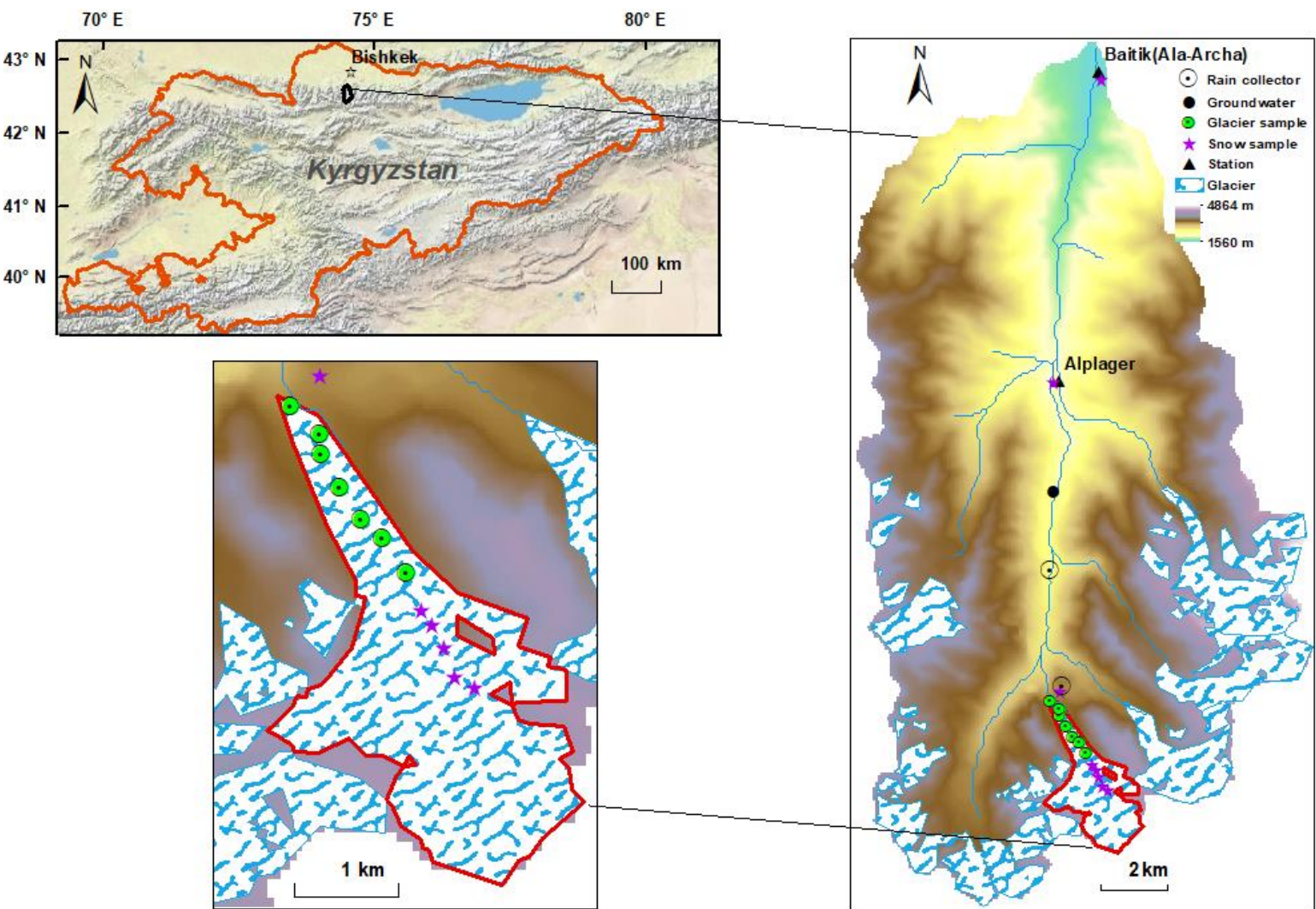
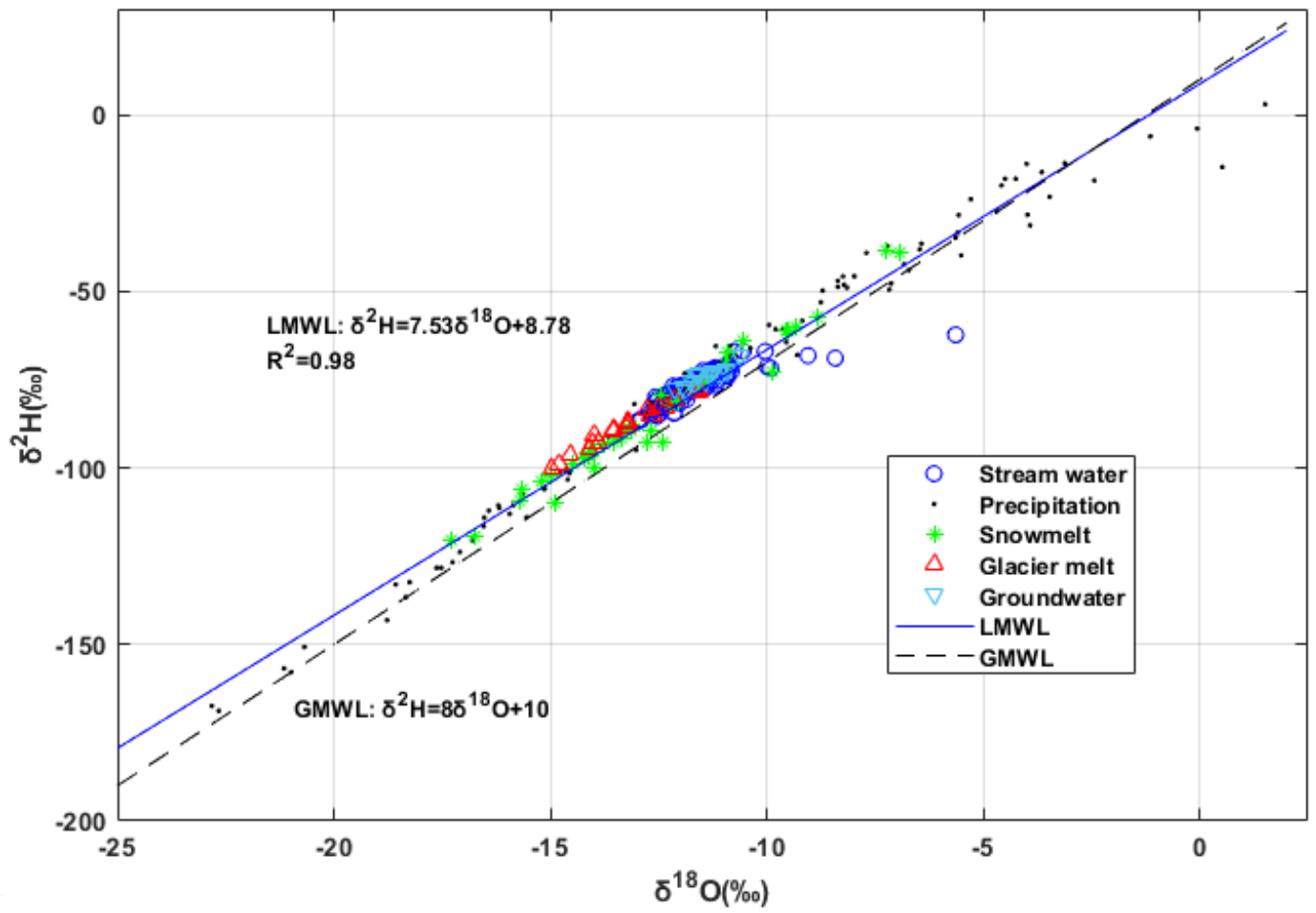
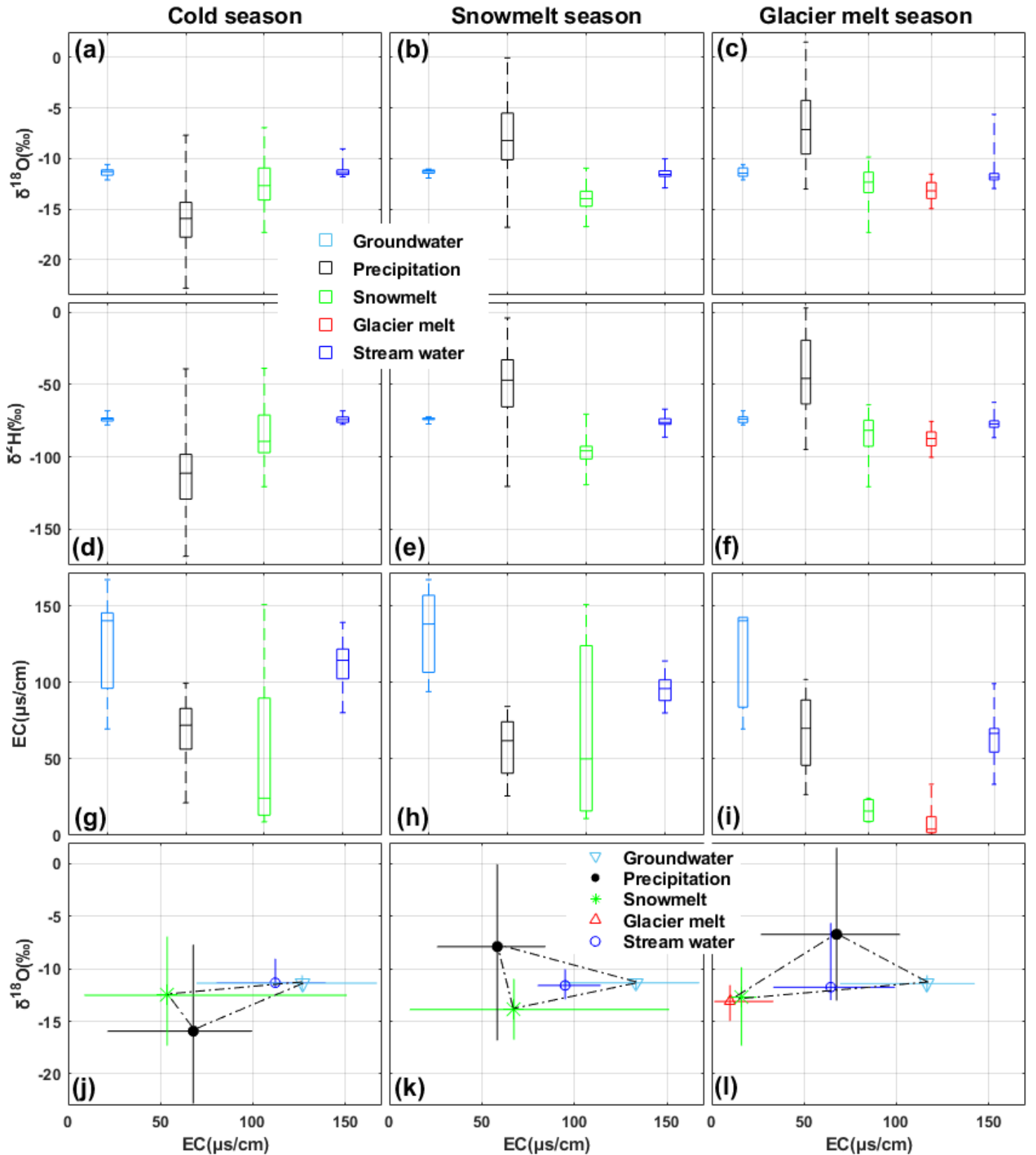


Figure 1. Study area of the Ala-Archa basin (derived from the ESRI World Topographic Map) and the Golubin Glacier including the locations of the water sampling points.



8

873 Figure 2. Isotope signatures of water samples from the three seasons in the Ala-Archa basin.



875 Figure 3. (a)-(i) Boxplots of tracer signatures in three seasons. (j)- (l) $\delta^{18}\text{O}$ -EC mixing space
 876 of the various water sources in the three seasons; the solid lines indicate the ranges of tracer
 877 signatures measured from water samples.

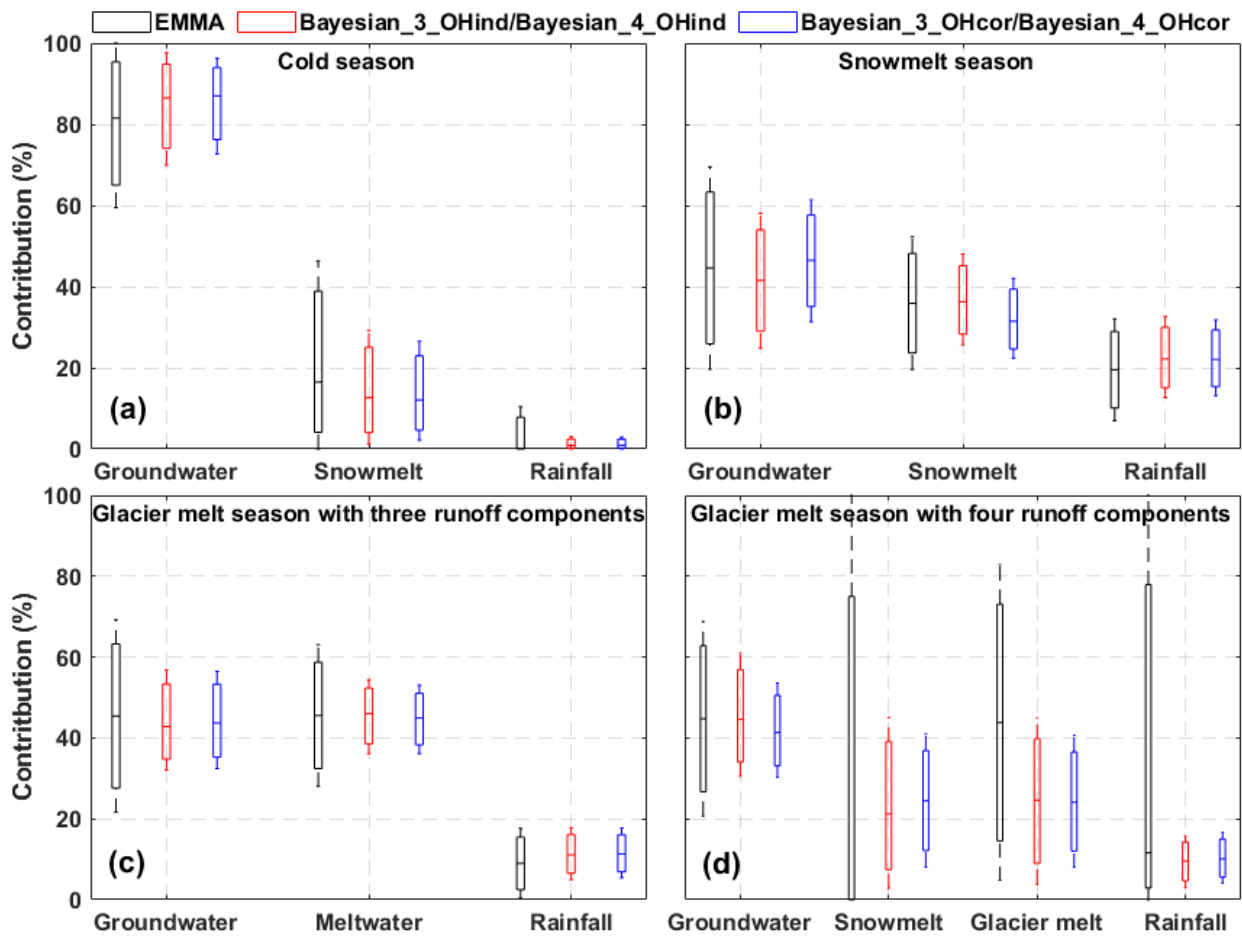


Figure 4. Contributions of runoff components (CRC) to total runoff estimated by different mixing approaches in three seasons. The Bayesian_3_OHind and Bayesian_3_OHcor were applied in the cold and melt seasons (a-c), and the Bayesian_4_OHind and Bayesian_4_OHcor were applied in the glacier melt season (d). The horizontal lines in the boxes refer to the median contributions, and whiskers refer to the 95% and 5% percentiles.

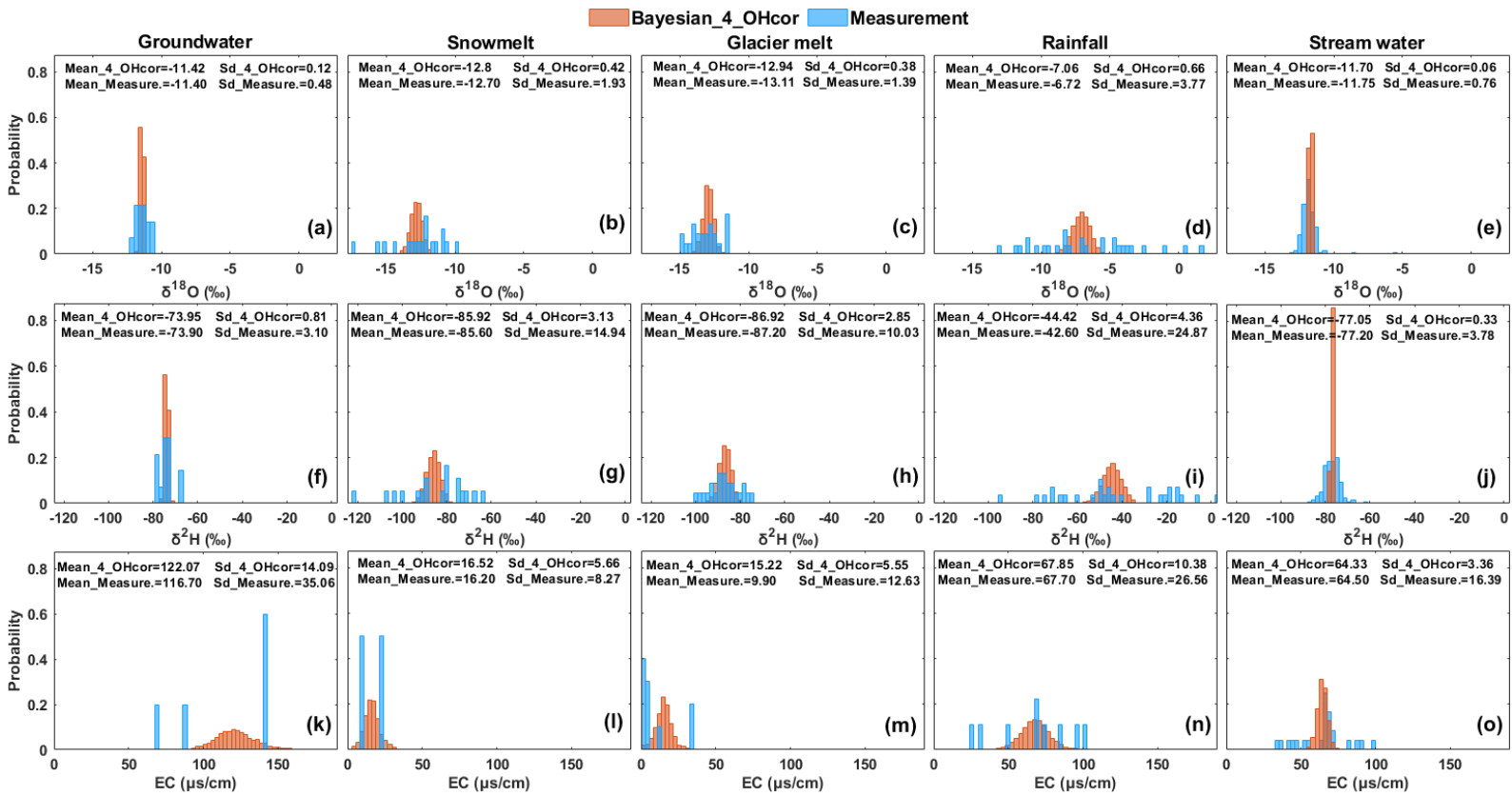
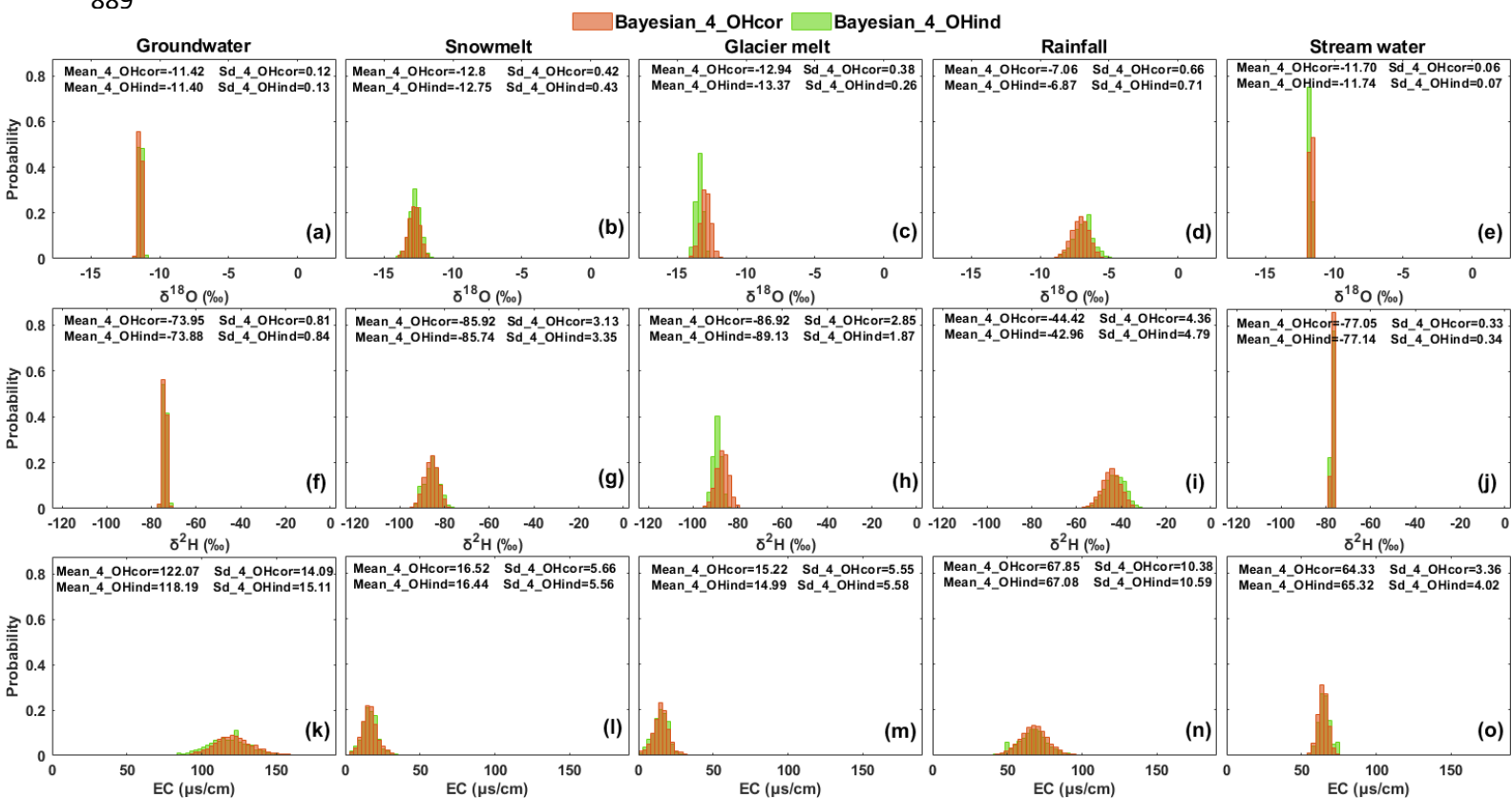
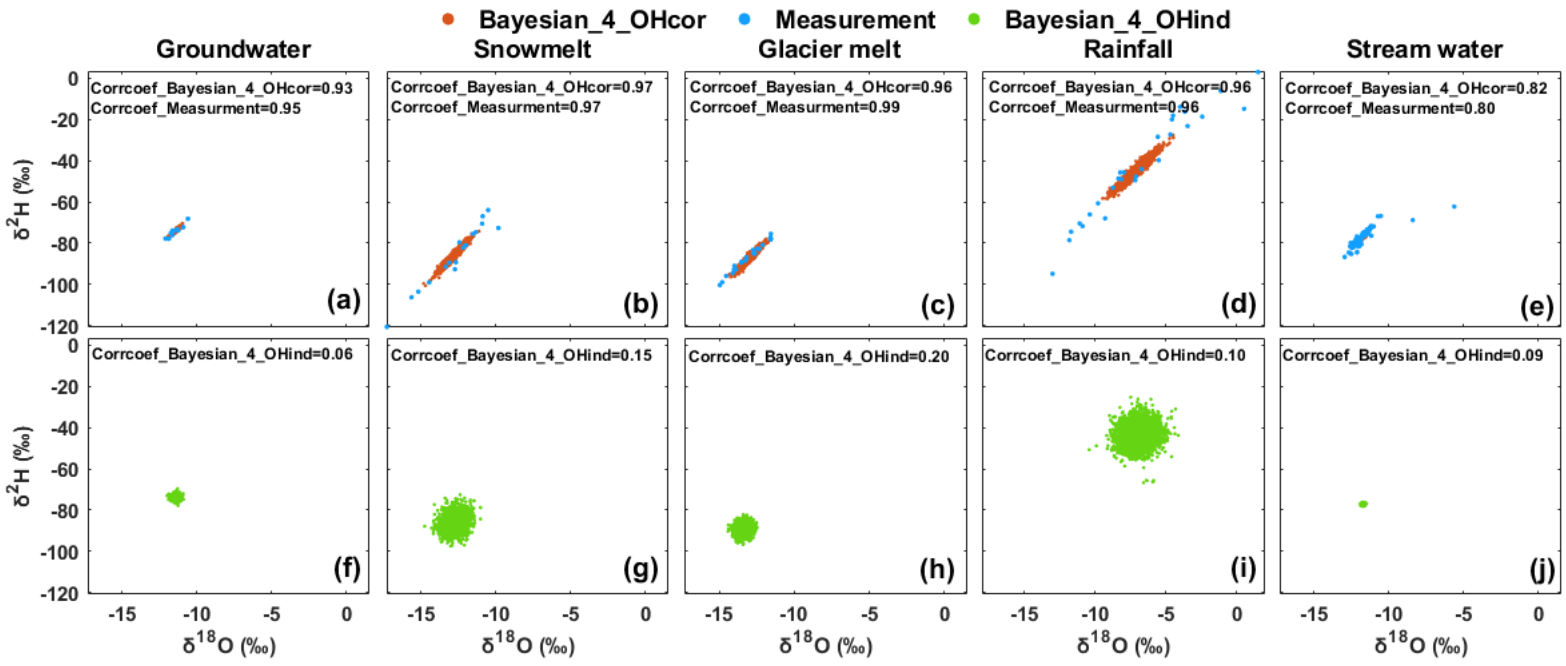


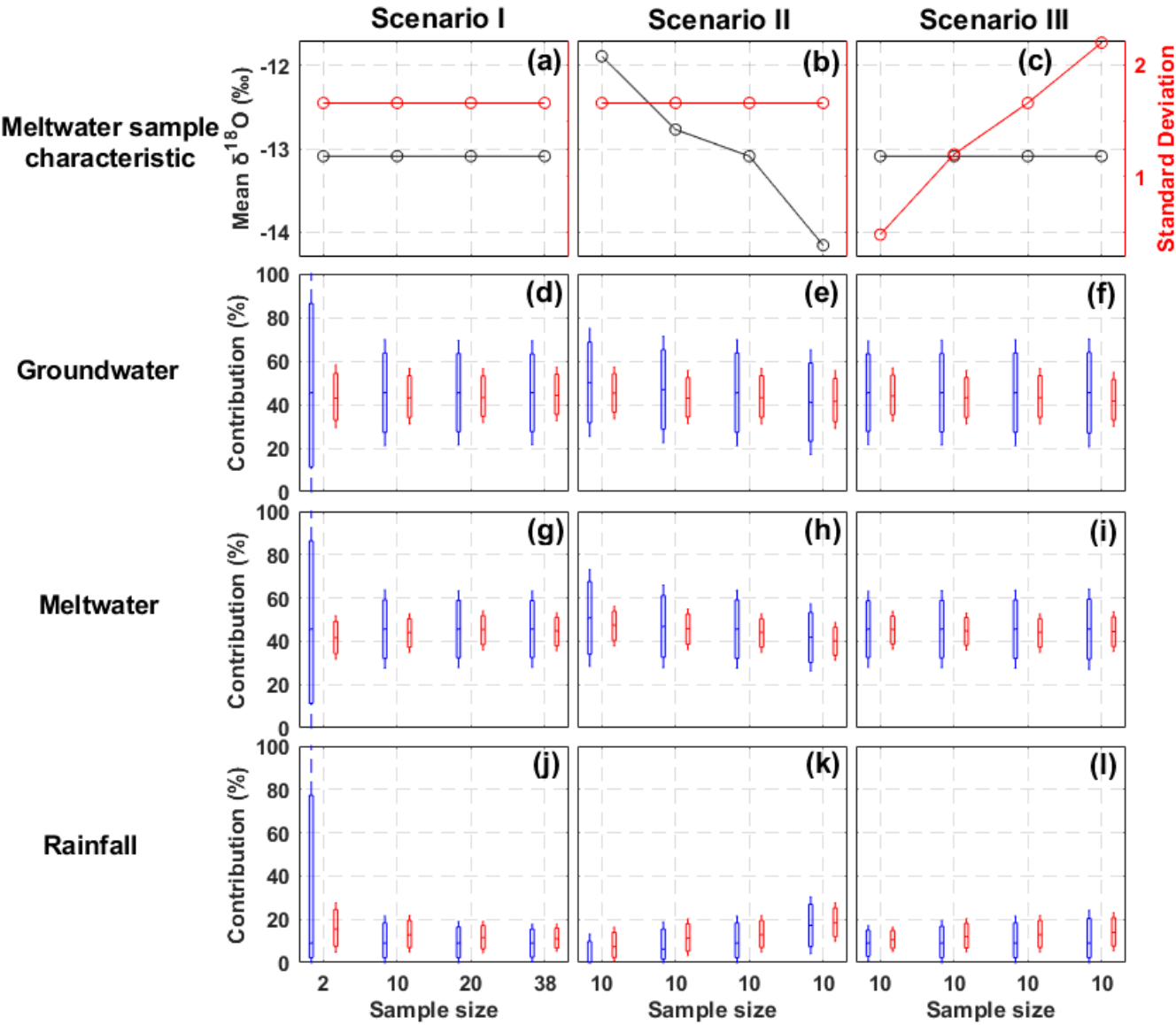
Figure 5. Posterior distributions of tracer signatures estimated by the Bayesian_4_OHcor in the glacier melt season. Measurement refers to the distributions of tracer signatures from the water samples. Row 1: distributions of $\delta^{18}\text{O}$; Row 2: distributions of $\delta^2\text{H}$; Row 3: distributions of EC.



891 Figure 6. Comparison of the posterior distributions of tracer signatures estimated by the
 892 Bayesian approaches with (Bayesian_4_OHcor) and without (Bayesian_4_OHind)
 893 considering the correlation between $\delta^{18}\text{O}$ and $\delta^2\text{H}$ in the glacier melt season.



895 Figure 7. Correlation between posterior $\delta^{18}\text{O}$ and $\delta^2\text{H}$ estimated by the Bayesian_4_OHcor
896 and the Bayesian_4_OHind approaches in the glacier melt season.



898

899

900

901

902

Figure 8. Sensitivity of the CRC estimates to the sample size (Scenario I), the mean (Scenario II) and standard deviation (Scenario III) of $\delta^{18}\text{O}$ of meltwater in the glacier melt season. Red boxes show the contributions estimated by the Bayesian_3_OHcor, and the blue boxes refer to the contributions estimated by the EMMA_3.

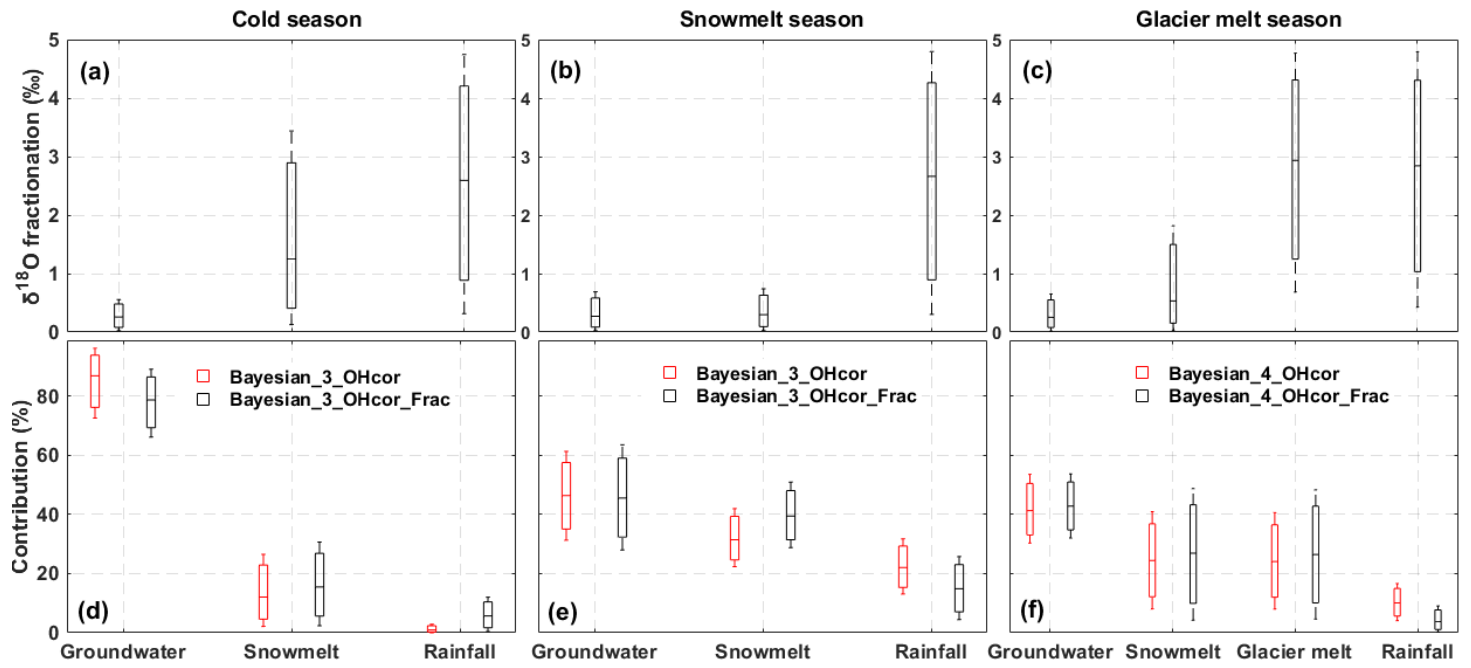


Figure 9. Effects of isotope fractionation on the estimates of CRC in the Bayesian approach for the three seasons. (a)-(c): Estimated changes in $\delta^{18}\text{O}$ of runoff components caused by the fractionation effect; (d)-(e): Comparison of the CRC estimated by the Bayesian_3_OHcor and the Bayesian_3_OHcor_Frac; (f): Comparison of the CRC estimated by the Bayesian_4_OHcor and the Bayesian_4_OHcor_Frac.

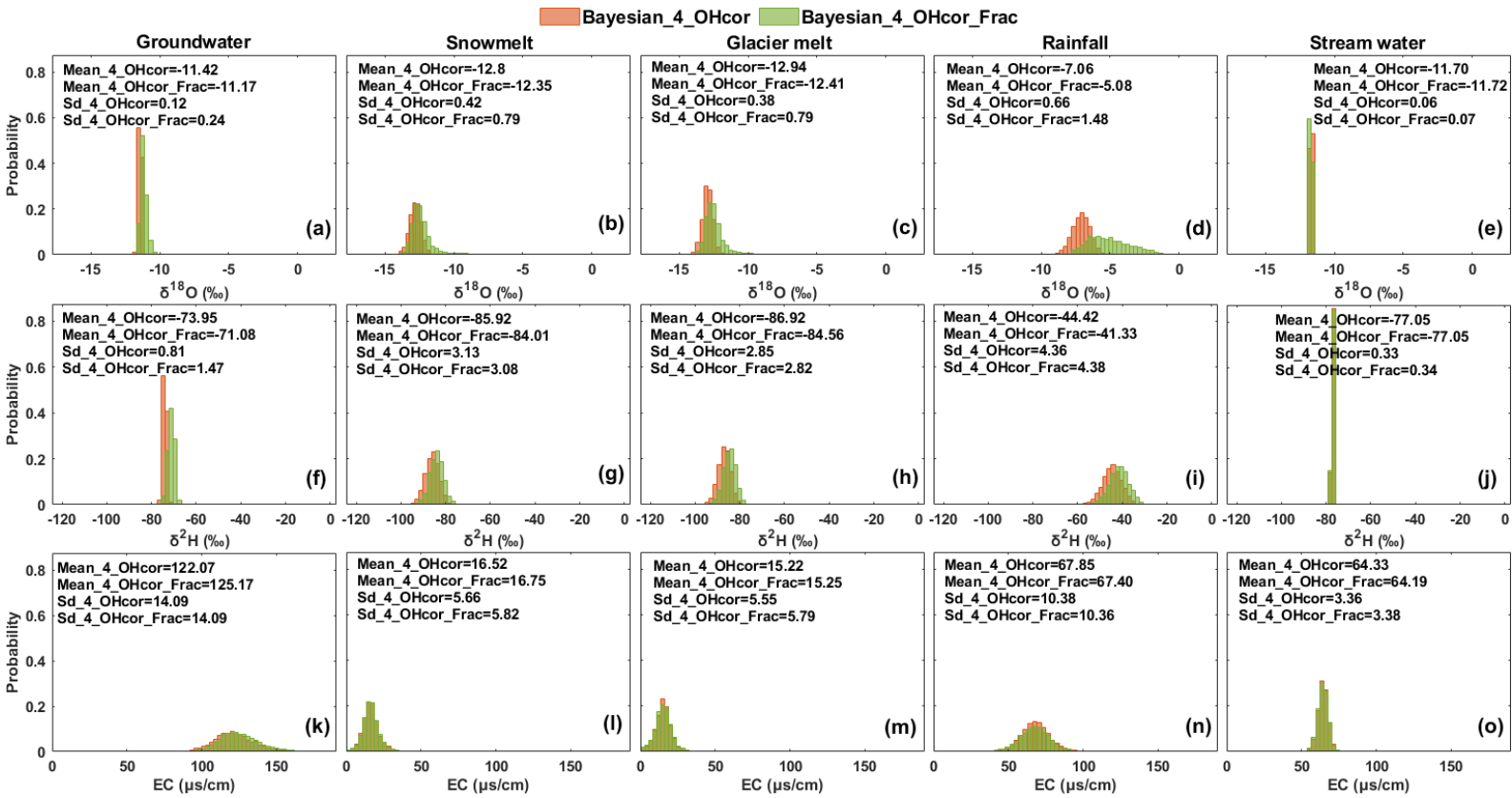


Figure 10. Effects of isotope fractionation on the posterior distributions of tracer signatures of water sources in the glacier melt season.